NUREG/CR-0880
HEDL-TME 79-29
RT

DYNAMIC ANALYSIS TO ESTABLISH NORMAL SHOCK AND VIBRATION OF RADIOACTIVE MATERIAL SHIPPING PACKAGES

QUARTERLY PROGRESS REPORT
JANUARY 1, 1979 - MARCH 31, 1979

Hanford Engineering Development Laboratory

HANFORD ENGINEERING DEVELOPMENT LABORATORY
Operated by Westinghouse Hanford Company
P.O. Box 1970 Richland, WA 99352
A Subsidiary of Westinghouse Electric Corporation
Prepared for the U.S. Nuclear Regulatory Commission
under Interagency Agreement DE-AC14-76FF02170
NRC FIN No. B2263-8

Available from
National Technical Information Service
Springfield, Virginia 22161

DISCLAIMER

NUREG/CR-0880
HEDL-TME 79-29
RT

DYNAMIC ANALYSIS TO ESTABLISH NORMAL SHOCK AND VIBRATION OF RADIOACTIVE MATERIAL SHIPPING PACKAGES

QUARTERLY PROGRESS REPORT
JANUARY 1, 1979 - MARCH 31, 1979

Hanford Engineering Development Laboratory

S. R. Fields
S. J. Mech

July 1979

HANFORD ENGINEERING DEVELOPMENT LABORATORY
Operated by Westinghouse Hanford Company
P.O. Box 1970 Richland, WA 99352
A Subsidiary of Westinghouse Electric Corporation
Prepared for the U.S. Nuclear Regulatory Commission
under Interagency Agreement DE-AC14-76FF02170
NRC FIN No. B2263-8

NUREG/CR-0880
HEDL-TME 79-29
RT

DYNAMIC ANALYSIS TO ESTABLISH NORMAL SHOCK AND VIBRATION OF RADIOACTIVE MATERIAL SHIPPING PACKAGES

Quarterly Progress Report
January 1, 1979 - March 31, 1979

S. R. Fields
S. J. Mech

ABSTRACT

This report represents work performed at the Hanford Engineering Development Laboratory operated by Westinghouse Hanford Company, a subsidiary of Westinghouse Electric Corporation, for the Nuclear Regulatory Commission, under Department of Energy Contract No. EY-76-C-14-2170. It describes technical progress made during the reporting period by Westinghouse Hanford Company and supporting contractors.

CONTENTS

FIGURES

FIGURES (Cont'd)

TABLES

NUREG/CR-0880
HEDL-TME 79-29
RT

DYNAMIC ANALYSIS TO ESTABLISH NORMAL SHOCK AND VIBRATION OF RADIOACTIVE MATERIAL SHIPPING PACKAGES

Quarterly Progress Report
January 1, 1979 - March 31, 1979

SUMMARY OF PROGRESS

1. DEVELOP DYNAMIC MODEL

The CARDS (Cask Rail-Car Dynamic Simulator) model was modified to account for the pitching moment caused by the application of a force through a coupler offset some small distance from a horizontal line through the center of gravity of the rail car. This term was added to the equation of motion defining the angle of rotation of the car.

2. DATA COLLECTION AND REDUCTION

Data recorded during the rail car impact tests conducted at the Savannah River Laboratories from July 14, 1978 through August 3, 1978 have been reduced and the initial analysis completed. This report presents additional results of the data reduction, and a cursory evaluation of the initial analysis. Results obtained using the spectral analysis technique are presented.

3. VALIDATE MODEL

A model validation algorithm to be incorporated into the CARDS model was tested successfully using the CARDT (Cask Rail-Car Dynamic Simulator Test) model. CARDT is a simple model designed to test modifications and additions to the more complex CARDS model.

The model validation algorithm is a statistical technique for computing a figure of merit from comparisons of time-varying values of predicted and actual outputs. The technique is based on Theil's inequality coefficients (TIC).

The algorithm was tested by comparing actual values of the time-varying coupler force, recorded following a 6-mile/hour impact between two 70-ton hopper cars loaded with gravel, with values calculated using the CARDT model. Results are presented as plots of coupler force and Theil's inequality coefficients as functions of time after impact.

5. PARAMETRIC AND SENSITIVITY ANALYSIS

A parametric and sensitivity analysis was initiated with the successful testing of one of two methods for the determination of parameter influence coefficients. The method tested is based on the computation of time-varying parameter influence coefficients (TPIC) during a simulation, using sets of

differential equations (sensitivity equations) derived from the equations of motion of the cask-rail car system. The TPIC method was tested using the CARDT model.

Calculated parameter influence coefficients are presented as functions of time after impact for the same simulation runs used to test the model validation algorithm.

6. INTERIM REPORT

An annotated videotape, prepared from high speed movies made during the cask-rail car humping tests conducted at the Savannah River Laboratories in July and August 1978, has been issued and is described in HEDL-TME 78-102.[1]

INTRODUCTION

This study was initiated in October 1977 as stated earlier in previous quarterly progress reports. The objective of this study is to determine the extent to which the shocks and vibrations experienced by radioactive material shipping packages during normal transport conditions are influenced by, or are sensitive to, various structural parameters of the transport system (i.e., package, package supports, and vehicle). The purpose of this effort is to identify those parameters which significantly affect the normal shock and vibration environments so as to provide the basis for determining the forces transmitted to radioactive material packages. Determination of these forces will provide the input data necessary for a broad range of package-tiedown structural assessments.

Progress on this study from January 1, 1979 to March 31, 1979 will now be discussed.

PROGRESS TO DATE

This study is divided into six tasks which have been discussed in previous progress reports. Progress on each of these tasks during this reporting period will now be discussed.

1. Develop Dynamic Model

The CARDS (Cask-Rail Car Dynamic Simulator) model was improved with the addition of a term representing the pitching moment caused by the offset of the coupler and the center of gravity of the rail car. This term was added to the equation of motion defining the angle of rotation of the car.

Figure 1, a simplified sketch of the rail car portion of the CARDS model, shows how the rotation of the rail car about a lateral axis passing through its center of gravity is enhanced by the moment of the coupler force about the axis. The moment about the center of gravity is

$$M_{RCCG} = Z_{CDG} DUSCAR \tag{1}$$

where

Z_{CDG} = the vertical distance between the line of force and the center of gravity (c.g.) of the rail car, inches

DUSCAR = the coupler force, lbs (force).

The coupler force is defined by

$$DUSCAR = k_{SCARS} (X_{RC} - X_F) \tag{2}$$

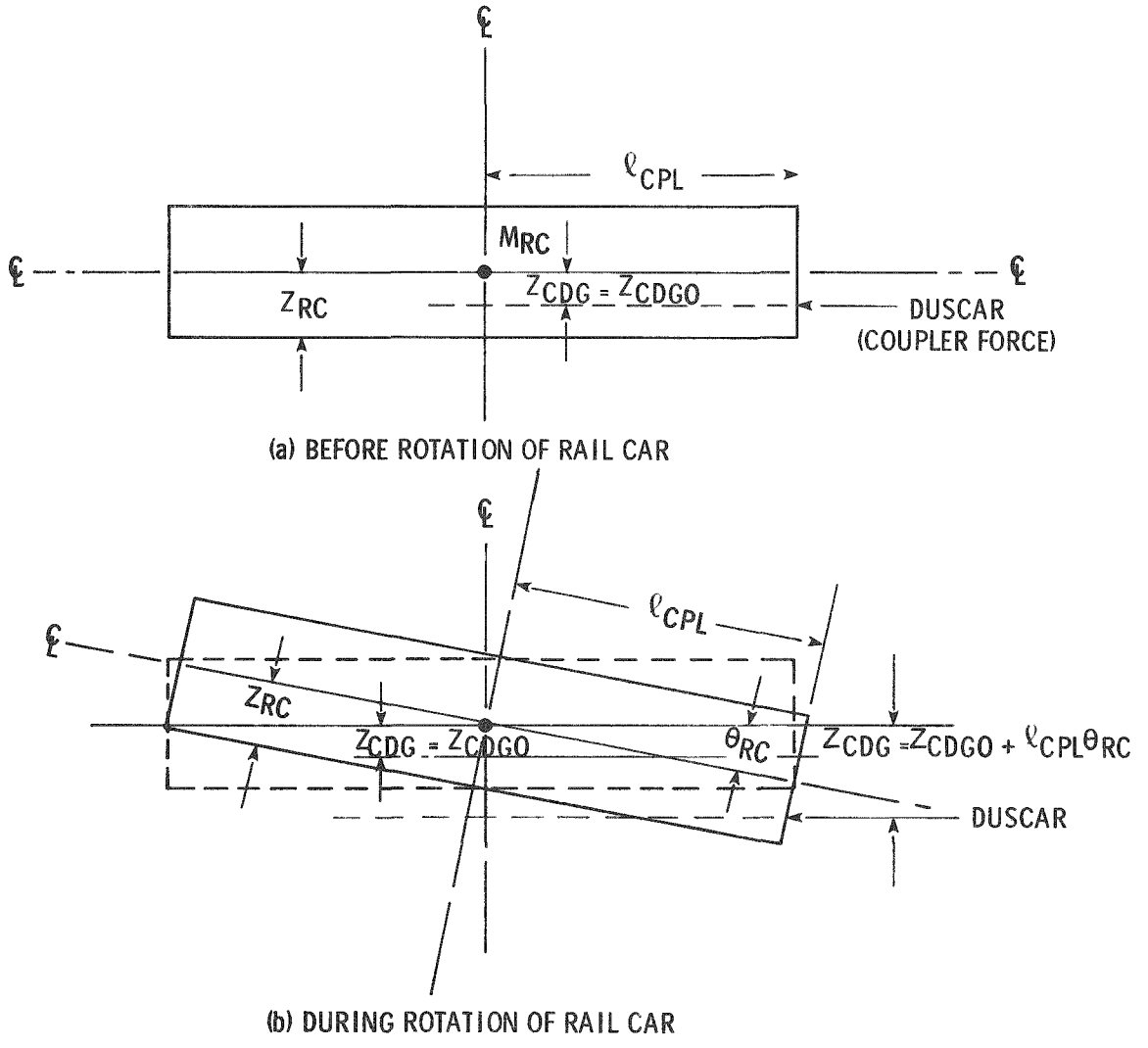

FIGURE 1. Effect of Coupler Offset on Rail Car Rotation.

where

k_{SCARS} = a total equivalent spring constant for the combined draft gears of the cask-rail car (hammer car) and the first struck car (anvil car), lbs (force)/inch (See Reference 1)

X_{RC} = the horizontal displacement of the c.g. of the cask-rail car, inches

X_F = the horizontal displacement of the c.g. of the first struck car, inches.

The vertical distance, Z_{CDG}, is defined by

$$Z_{CDG} = Z_{CDGO} + l_{CPL}\,\theta_{RC} \tag{3}$$

where

Z_{CDGO} = the distance between the centerline of the draft gear and the center of gravity of the cask-rail car, inches

l_{CPL} = the horizontal distance from the vertical centerline of the cask-rail car to the coupler face, inches

θ_{RC} = the angle of rotation of the cask-rail car about the lateral axis through its center of gravity, radians.

The pitching moment, M_{RCCG}, was added to the equation of motion that defines the angle of rotation of the cask-rail car, i.e.,

$$\frac{d^2\theta_{RC}}{dt^2} = \frac{\left\{ \sum_i^N \left[\left(DUS_i \right) \left(l_i \right) \right] + M_{RCCG} \right\}}{I_{RC}} \tag{4}$$

where

DUS_i = the i-th force on the rail car, lbs (force)

l_i = the distance from the rail car c.g. to the line of the applied i-th force, inches.

2. Data Collection and Reduction

Data recorded during the experimental tests at Savannah River Laboratories (see Table 2 of Reference 1) have been reduced and the initial analysis completed. This report will cover the recovered and reduced data channels as well as cursory evaluation of the initial analysis.

Table 1 is a tabulation of the data channels which have been transcribed and reduced. This tabulation refers to the instrument numbers defined in Table 2 (Table 3 of Reference 1). Table 1 defines unique identification codes employed during reduction and subsequent analysis. To date, the data reduction for each channel of information consists of measuring the maximum and minimum instant values of the time-domain data, and converting these data to the corresponding frequency spectra by Fast Fourier Transforms (FFT). As previously discussed,[2] it is this frequency domain information which will permit comparison of experimental data, and assist in validating the analytical model.

As a demonstration of the spectral analysis technique, the vertical acceleration on the struck end of the cask (Instrument 9) is presented in Figures 2 through 9 for the following tests and conditions.

TABLE 1

DATA CHANNEL IDENTIFICATION AND STATUS

INST No.	Test 1	Test 2	Test 3
1	1B	2B2*	3B2
2	1C	NC	NC
3	1B2*	2B	3B
4	1A, 1A2*	2A, 2A2*	3A1, 3A2*
5	1H2*	2H2*	3H2*
6	1J2*	2J2*	3J2*
7	1K2*	2K2*	3K2*
8	1D	2D	3D
9	1E	2E	3E
10	1F	2F	3F
11	1G	2G	3G
12	1H	2H	3H
13	1J	2J	3J
14	1K	2K	3K
15	1C2*	2C2*	3C2*
16	1D2*	2D2*	CL
17	1L	2L	3N2*
18	DISP	DISP	DISP
19	1E2*	2E2*	3E2*
20	1F2*	2F2*	3F2*
21	IRIG	IRIG	IRIG
22	1M	2M	3M
23	1G2*	2G2*	3G2*
24	1L2*	2L2*	3L2*
25	IRIG	IRIG	IRIG
26	1N	2N	3N
27	1M2*	2M2*	3C
28	1N2*	2N2*	3L

TABLE 1 (Cont'd)

INST No.	Test 4	Test 5	Test 10
1	4B2	5B2*	10B
2	NC	NC	NC
3	4B	5B	10B2
4	4A, 4A2	5A*, 5A2	10A, 10A2
5	4H2	5H2	10H
6	4J2	5J2	HJ
7	4K2	5K2	10K
8	4D	5D*	10D2
9	4E	5E*	10E2*
10	4F	5F*	10F2
11	4G	5G*	10G2
12	4H	5H*	10H2
13	4J	5J*	10J2
14	4K	5K*	10K2
15	CL	CL	10C
16	CL	CL	10D
17	4N2	5N2	10N
18	DISP	DISP	DISP
19	4E2	5E2	10E
20	4F2	5F2	10F
21	IRIG	IRIG	IRIG
22	4M	5M*	10M2
23	4G2	5G2	10G
24	4L2	5L2	10L
25	IRIG	IRIG	IRIG
26	4N	5N*	DISP
27	4C	5C*	10C2
28	4L	5L*	10L2

TABLE 1 (Cont'd)

INST No.	Test 11	Test 13
1	11B	DISP
2	NC	NC
3	11B2	13B
4	11A, 11A2	13A, 13A2
5	11H	13H2
6	11J	13J2
7	11K	13K2
8	11D2	13D
9	11E2*	13E
10	11F2*	13F
11	11G2	13G
13	11J2	13J
14	11K2	13K
15	11C	13C2
16	11D	13D2
17	11N	13N*
18	11N2	13M2
19	11E	13E2
20	11F	13F2
21	IRIG	IRIG
22	11M2	13M
23	11G	13G2
24	11L	13L2
25	IRIG	IRIG
26	DISP	DISP
27	11C2	13C
28	11L2	13L*

TABLE 1 (Cont'd)

INST No.	Test 16	Test 17	Test 18
1	DISP	DISP	DISP
2	NC	NC	NC
3	16B2	17B2	18B2
4	16A, 16A2	17A, 17A2	18A, 17A2
5	16H	17H	18H
6	16J	17J	18J
7	16K	17K	18K
8	16D2	17D2	18D2
9	16E2	17E2	18E2
10	16F2	17F2	18F2
11	16G2	17G2	18G2
12	16H2	17H2	18H2
13	16J2	17J2	18J2
14	16K2	17K2	18K2
15	16C	17C	18C
16	16D	17D	18D
17	16N2*	17N2*	18N2*
18	16M*	17M*	18M*
19	16E	17E	18E
20	16G	17F	18F
21	IRIG	IRIG	IRIG
22	16M2	17M2	18M2
23	16G	17G	18G
24	16L	17L	18L
25	IRIG	IRIG	IRIG
26	16B	17B	18B
27	16C2	17C2	18C2
28	16L2	17L2	18L2

* = DATA BEING RECHECKED DUE TO POSSIBLE TRANSLATION ERRORS

NC = NOT COMPLETED

CL = CLIPPED SIGNAL

IRIG = TRACK USED FOR TIMING

DISP = TRACK USED FOR DISPLACEMENT (DATA CORRELATION)

TABLE 2

INSTRUMENT CONFIGURATION FOR CASK-RAIL CAR-TIEDOWN TESTS

CONFIGURATIONS A AND B

Instrument No.	Instrument Location	Instrument Type	Measurements
1	Bolt Holddown (FE)*	Instrumented Bolt	Change in Tension
2	Bolt Holddown (Side)	Instrumented Bolt	Change in Tension
3	Coupler	Bridge Type	Force/Time
4	Struck End of Car	Displacement	Displacement/Time
5	Car Structure (SE)*	PR Accelerator	Shock
6	Car Structure (SE)	PR Accelerator	↓
7	Car Structure (SE)	PE Accelerator	↓
8	Cask (SE)	PR Accelerator	↓
9	Cask (SE)	PR Accelerator	↓
10	Cask (FE)	PR Accelerator	↓
11	Cask (FE)	PR Accelerator	↓
12	Car/Cask Interface	PR Accelerator	↓
13	Car/Cask Interface	PR Accelerator	↓
14	Car/Cask Interface	PR Accelerator	↓
15	Cask Base (SE)	PE Accelerator	↓
16	Cask Base (SE)	PE Accelerator	↓
17	Cask Base (FE)	PE Accelerator	↓
18	Cask Base (FE)	PE Accelerator	↓
19	Cask Top Center	PE Accelerator	↓
20	Cask Side Center	PE Accelerator	↓
21	Car Structure (FE)	PE Accelerator	Shock
22	Car Structure (FE)	PE Accelerator	Shock
23	Truck (SE)	PE Accelerator	Shock
24	Truck (FE)	PE Accelerator	Shock
25	Rail Car Above Truck Center (SE)	PE Accelerator	Shock
26	Bolted Holddown (FE)	Instrumented Bolt	Change in Tension
27	Base/Chock Interface (SE)	Load Cell	Change in Compression
28	Base/Chock Interface (SE)	Load Cell	Change in Compression

*SE = STRUCK END
FE = FAR END

TABLE 2 (Cont'd)

CONFIGURATIONS* C** AND D

Instrument No.	Instrument Location	Instrument Type	Measurements
1	Cable (FE)*	Load Cell	Change in Tension
2			
3	Coupler	Bridge Type	Force/Time
4	Struck End of Car	Displacement	Displacement/Time
5	Car Structure (SE)*	PR Accelerator	Shock
6	Car Structure (SE)	PR Accelerator	
7	Car Structure (SE)	PE Accelerator	
8	Cask (SE)	PR Accelerator	
9	Cask (SE)	PR Accelerator	
10	Cask (FE)	PR Accelerator	
11	Cask (FE)	PR Accelerator	
12	Car/Cask Interface	PR Accelerator	
13	Car/Cask Interface	PR Accelerator	
14	Car/Cask Interface	PE Accelerator	
15	Cask Base (SE)	PE Accelerator	
16	Cask Base (SE)	PE Accelerator	
17	Cask Base (FE)	PE Accelerator	
18	Cask Base (FE)	PE Accelerator	
19	Cask Top Center	PE Accelerator	
20	Cask Side Center	PE Accelerator	
21	Car Structure (FE)	PE Accelerator	
22	Rail Car Above Truck Center (FE)	PE Accelerator	Shock
23	Truck (SE)	PE Accelerator	Shock
24	Truck (FE)	PE Accelerator	Shock
25	Rail Car Above Truck Center (SE)	PE Accelereator	Shock
26	Cable (FE)	Load Cell	Change in Tension
27	Base/Chock Interface (SE)	Load Cell	Change in Compression
28	Base/Chock Interface (SE)	Load Cell	Change in Compression

*SE = STRUCK END **Only Instrument No's 1, 3 and 26 on Configuration C.
FE = FAR END

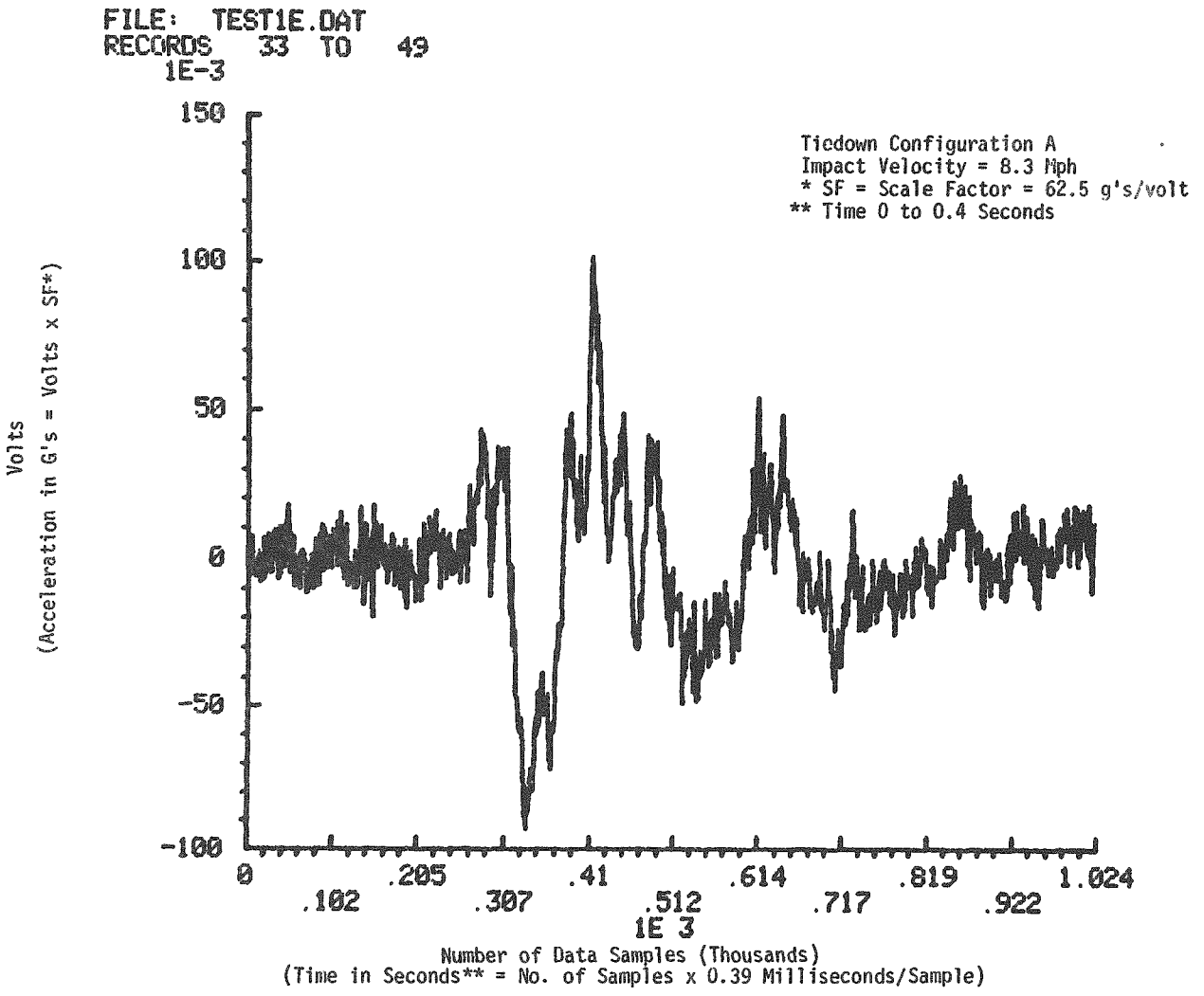

FIGURE 2. Vertical Acceleration of Cask at Struck End vs Time During Test 1E (Instrument No. 9 - Unfiltered).

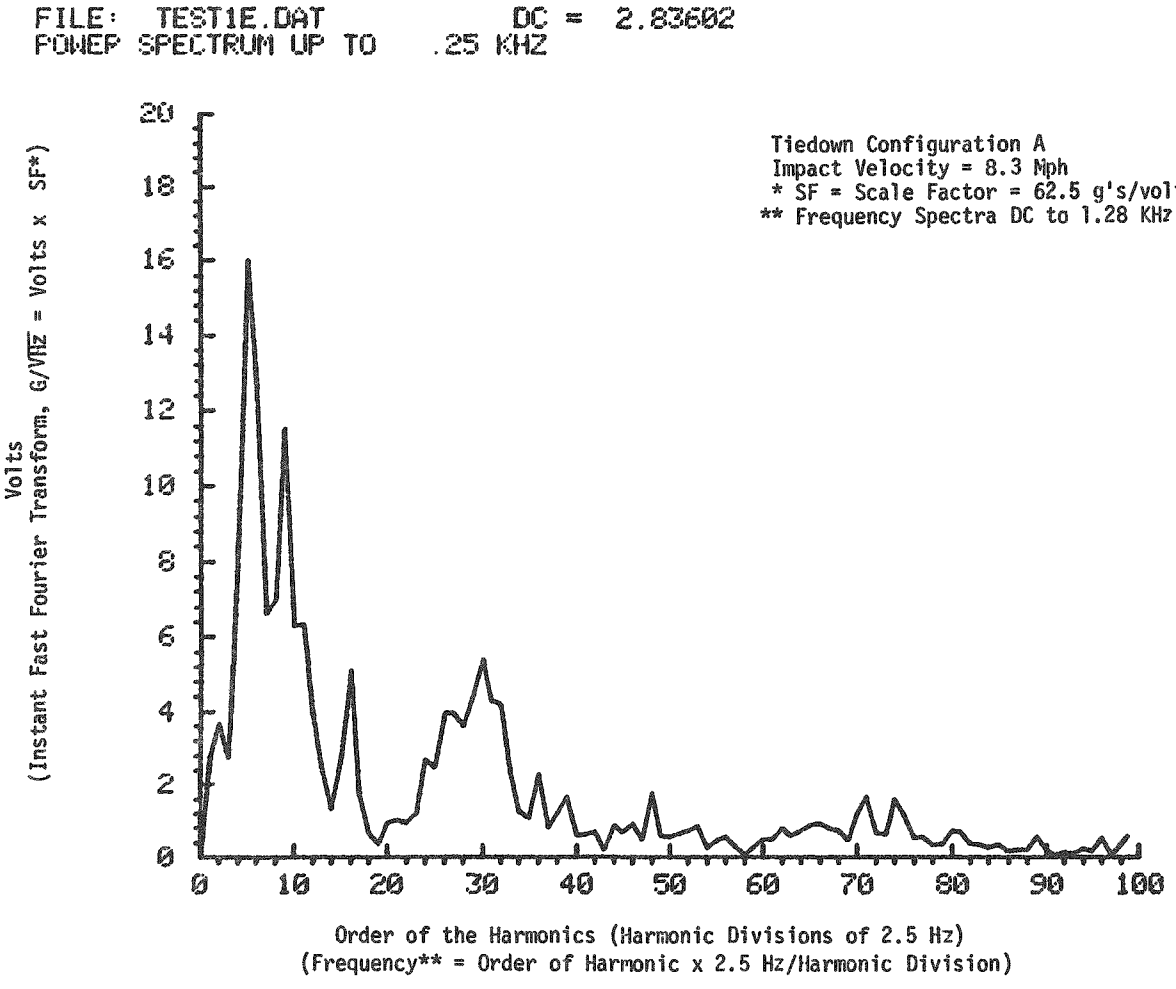

FIGURE 3. Vertical Acceleration Response of Cask at Struck End vs Frequency for Test 1E (Instrument No 9 - Unfiltered).

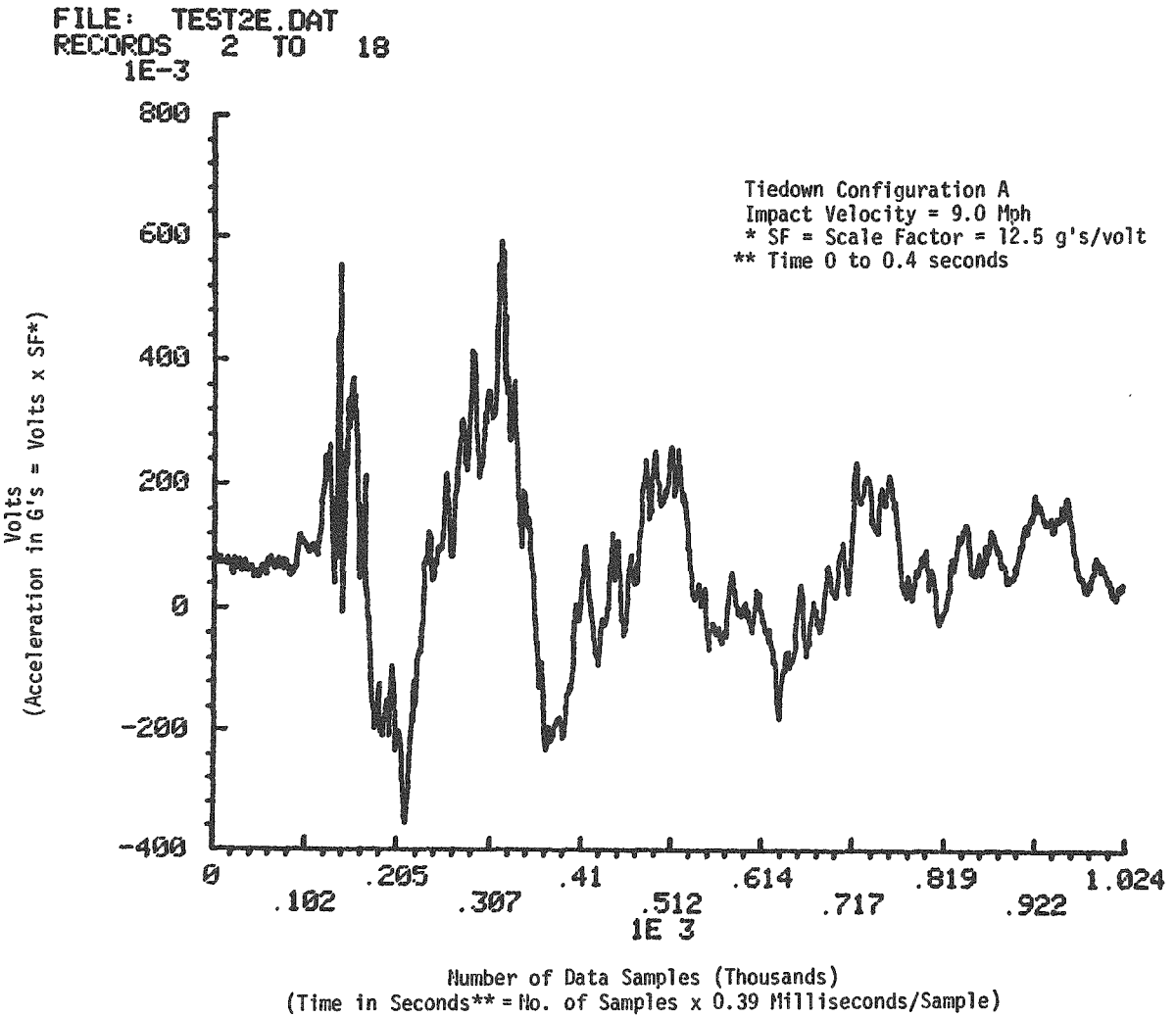

FIGURE 4. Vertical Acceleration of Cask at Struck End vs Time During Test 2E (Instrument No. 9 - Unfiltered).

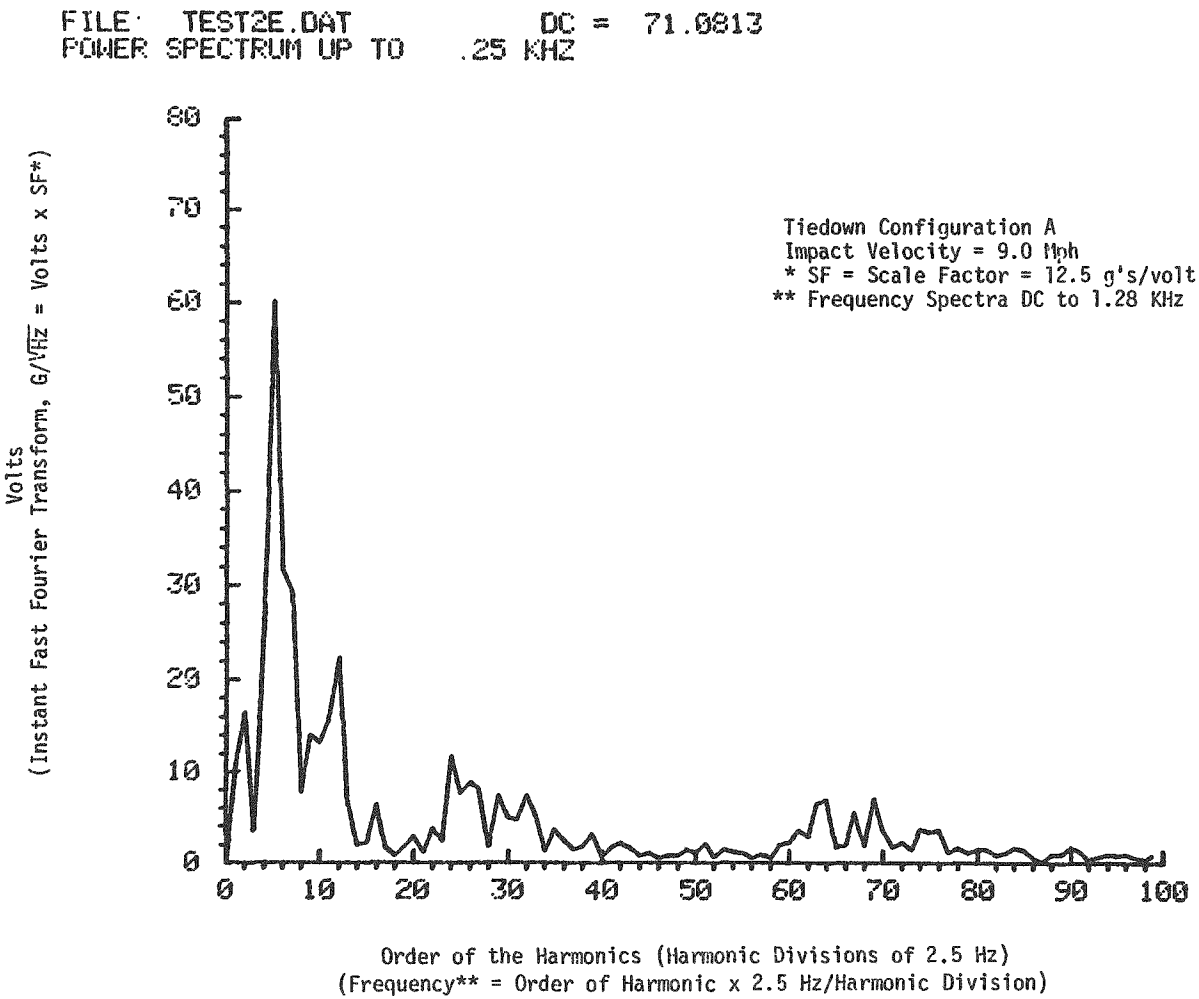

FIGURE 5. Vertical Acceleration of Cask at Struck End vs Frequency for Test 2E (Instrument No. 9 - Unfiltered).

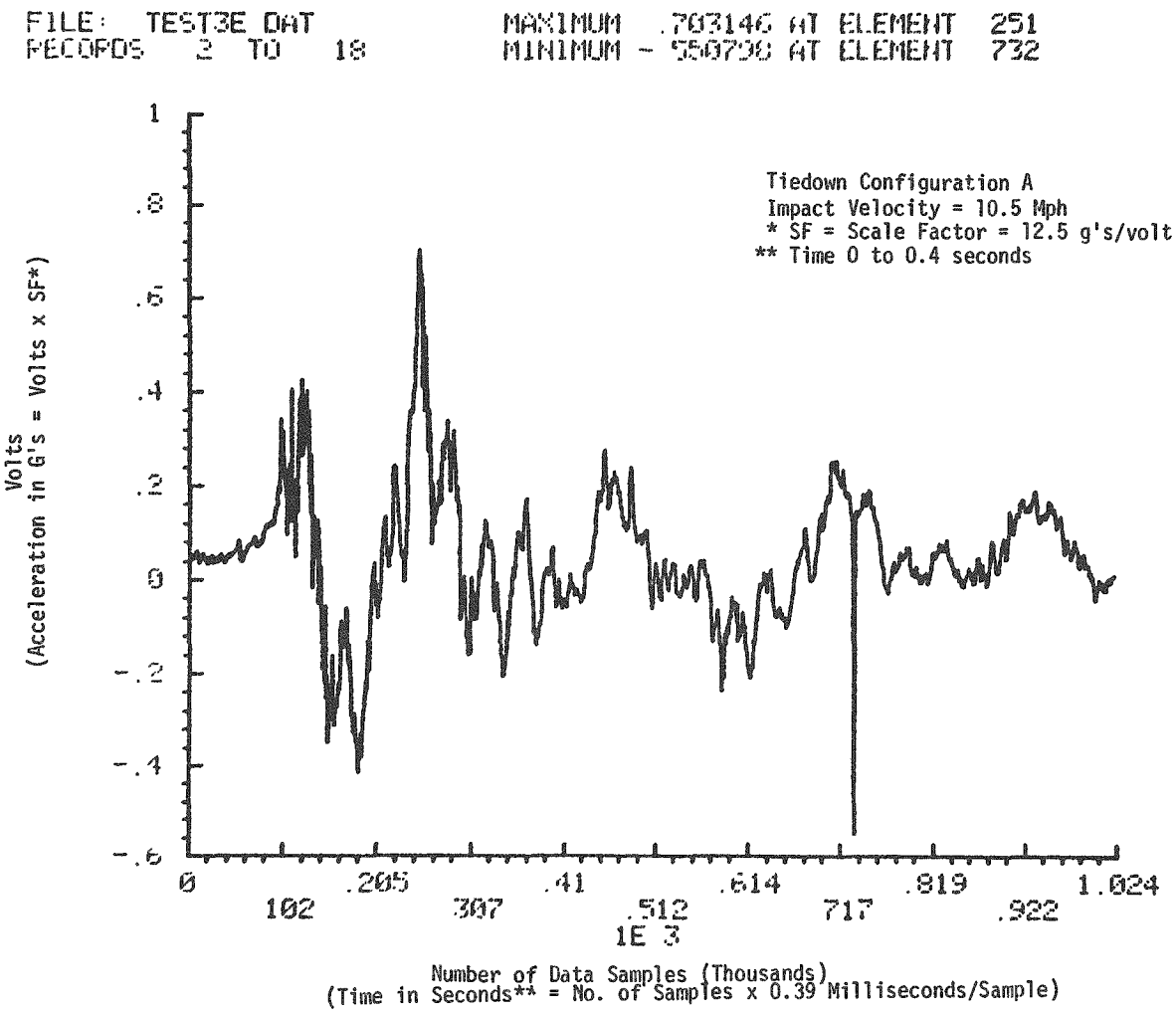

FIGURE 6. Vertical Acceleration of Cask at Struck End vs Time During Test 3E (Instrument No. 9 - Unfiltered).

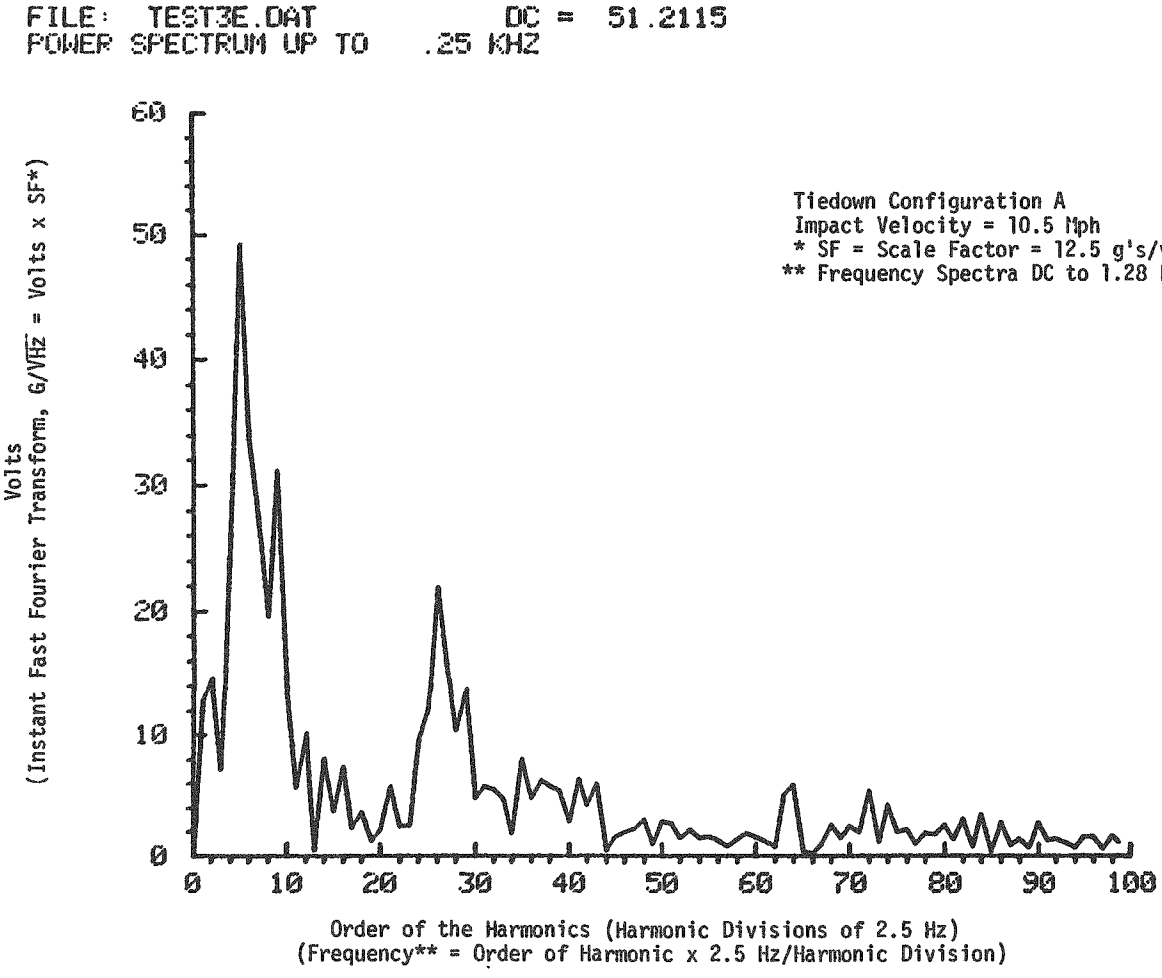

FIGURE 7. Vertical Acceleration of Cask at Struck End vs Frequency for Test 3E (Instrument No. 9 - Unfiltered).

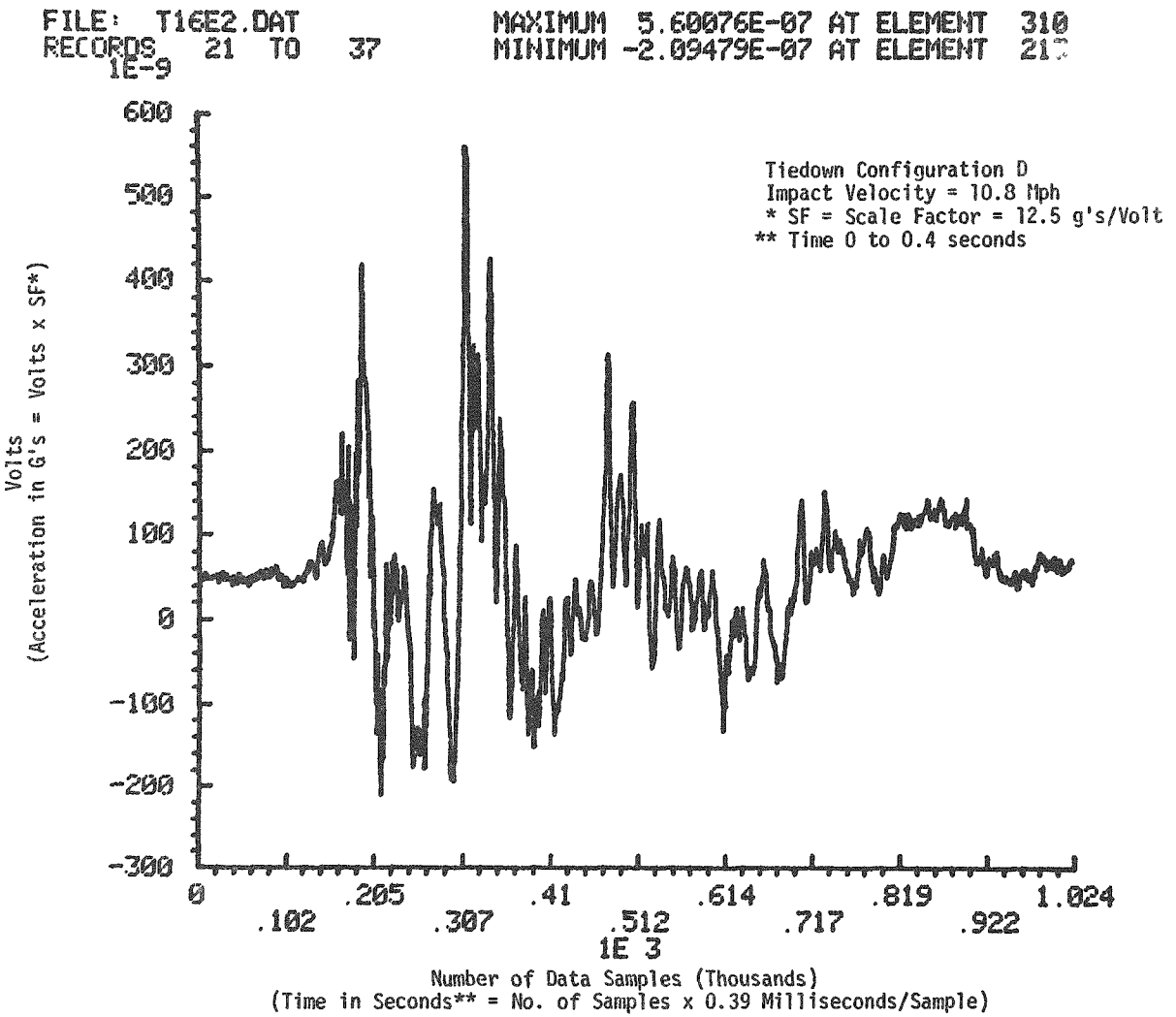

FIGURE 8. Vertical Acceleration of Cask at Struck End vs Time During Test 16E (Instrument 9 - Unfiltered).

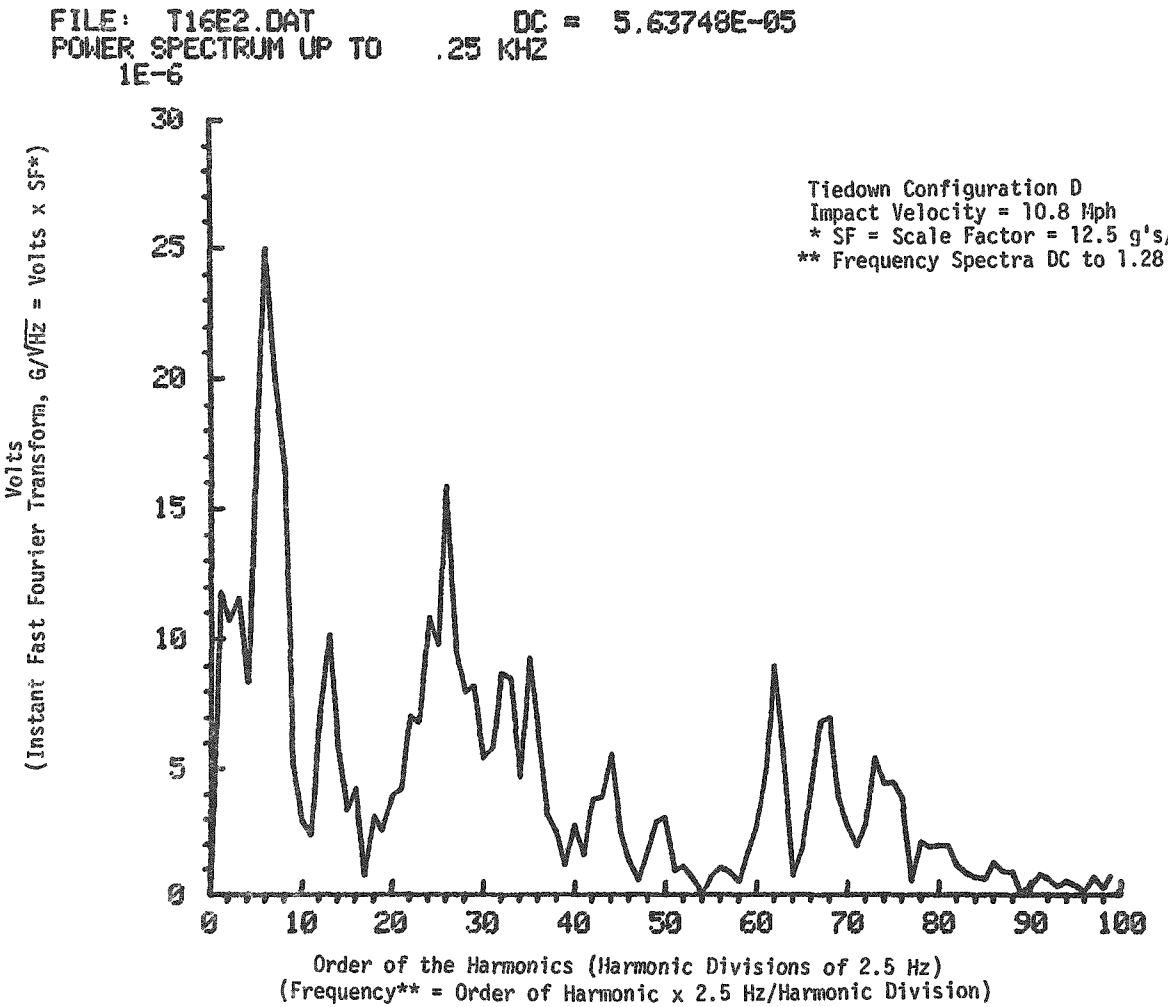

FIGURE 9. Vertical Acceleration of Cask at Struck End vs Frequency for Test 16E (Instrument No. 9 - Unfiltered).

Test	Tiedown Configuration	Impact Velocity (mph)	Scale Factor SF (g's/volt)
1	A	8.3	62.5
2	A	9.0	12.5
3	A	10.5	12.5
16	D	10.8	12.5

Recalling that the tiedown support was changed between tests 1 and 2, and that sensitivity (i.e., scale factor) on the selected channel was modified by a factor of five, the time domain waveforms (Figures 2 and 4) appear similar in peak amplitude; but there are variations in the spectral information (Figures 3 and 5). Comparison of Tests 2 and 3 reveals the expected increase in peak time domain amplitude with speed (Figures 4 and 6), yet the power spectra has a lowered peak amplitude with an apparent energy shift to the third harmonic of that peak (Figures 5 and 7). Test 16, a cable tie-down configuration, shows little time domain similarity to Test 3 which is at a comparable speed and scale factor (Figures 6 and 8); however, their power spectra may possibly be comparable with appropriate scaling (Figures 7 and 9).

Although empirical methods of comparisons have been employed in this demonstration, analytical methods such as Theil's inequality coefficients (see Section 3) will be used later for data comparison and model validation. The purpose of including this informal analysis here was to illustrate that comparison of time domain information does not reflect energy content, as does the spectral information. It is the latter domain which has the greater potential for model and data validation.

During the next quarter, efforts will be made to verify data that are questionable and to analytically employ experimental data to verify the model.

3. Validate Model

A model validation algorithm to be incorporated into the CARDS model has been tested using the CARDT (Cask Rail Car Dynamic Simulator Test) model, the simple cask-rail car coupler subsystem model described in Reference 1. This simple model has been used frequently to test and perfect modifications and additions to the more complex CARDS model. CARDT was also used during this reporting period to test a method for determining parameter influence coefficients simultaneously with the solution of the equations of motion (see Section 5).

The model validation algorithm used is a statistical technique for computing a figure of merit from comparisons of time-varying values (series) of predicted and actual outputs. Statistical techniques available for testing the "goodness" of fit of models to actual system behavior include analysis of variance, the Chi-square test, factor analysis, Kolmogorov-Smirnov tests, nonparametric test, regression analysis, spectral analysis, and Theil's inequality coefficients.[3] The technique based on Theil's inequality coefficients has been programmed into CARDT and demonstrated successfully, and will be included in the CARDS model soon. This technique was chosen as one of two model validation algorithms to be used for three reasons:

(1) It represents a simple addition to the dynamic model,

(2) It produces one number or figure of merit (the inequality coefficient) which reflects the degree of agreement between the model and the system modeled, and

(3) It may be expanded to measure the degree of agreement based on "n" output variables by using Theil's multiple inequality coefficient.

The second model validation algorithm chosen for use with the CARDS model is based on spectral analysis. This algorithm was transformed into the computer program FFT (Fast Fourier Transform) as part of the data collection and reduction task. FFT converts the displacement, velocity and acceleration response of a cask-rail car system from the time domain to the frequency domain, and allows the response spectra to be determined directly from either model output or from test data. Examples of response spectra produced by FFT from test data have been presented in Figures 14 through 19 of the previous progress report[4], and in Figures 3, 5, 7 and 9 of the present report. Additional work is now in progress to convert preliminary output from the CARDS model, and additional test data, from the time domain to the frequency domain. Originally, it was intended that FFT would be used as a subroutine in the CARDS model; but, due to certain incompatibilities with ACSL (Advanced Continuous Simulation Language), it is used instead as a separate program for processing model output as if it were the recorded output from an experiment.

Theil's inequality coefficient is defined as

$$TIC = \frac{\left[\frac{1}{n}\sum_{i}^{n}(Y_{Pi} - Y_{Ai})^2\right]^{0.5}}{\left(\frac{1}{n}\sum_{i}^{n}Y_{Pi}^2\right)^{0.5} + \left(\frac{1}{n}\sum_{i}^{n}Y_{Ai}^2\right)^{0.5}} \qquad (5)$$

where n is the number of sampling points, and

$$Y_{P1}, Y_{P2}, Y_{P3}, \ldots\ldots, Y_{Pi}, \ldots\ldots, Y_{Pn}$$
$$Y_{A1}, Y_{A2}, Y_{A3}, \ldots\ldots, Y_{Ai}, \ldots\ldots, Y_{An}$$

are the values of an output variable Y at discrete points in time (a time series). Y_{Pi} and Y_{Ai} are the corresponding predicted and actual values, respectively, of the output variable Y. The values of TIC from Equation (5) will vary between the following two extremes:

TIC = 0 when $Y_{Pi} = Y_{Ai}$ for all i
(The case of equality or perfect agreement)

TIC = 1 (The case of maximum inequality or poor agreement).

Theil's multiple or overall inequality coefficient (TMIC) is a figure of merit based on the number of observations, the values of several output variables selected at discrete points, and the two-variable inequality coefficients defined by Equation (5). The two-variable coefficients are combined in a prescribed manner to generate the TMIC.[3]

The model validation algorithm based on Theil's inequality coefficients (TIC) was tested by comparing actual values of the time-varying coupler force, recorded following a 6-mile/hour impact between two 70-ton hopper cars loaded with gravel,[5] with values calculated using the CARDT model. Results from the impact test were reported by Baillie[5] and presented in Figures 3 and 4 of Reference 1. For convenience, these figures are presented here as Figures 10 and 11. These figures also show the coupler force calculated by the CARDT model as a function of time during impact, for "solid" draft gear spring constants of 5×10^5 lbs(force)/inch and 1×10^6 lbs(force)/inch, respectively. The "solid" state of a draft gear refers to that state after bottoming out when it behaves as a solid beam. This is in contrast to the "active" state, the normal condition before the draft gear spring has reached its limit of travel. The spikes at the center of each plot represent the coupler force during the solid state while the ramps on each side of the spikes represent the coupler force during the active state. Theil's inequality coefficient (TIC), the figure of merit calculated by CARDT to show the degree of agreement between the model and the actual system, is presented as a function of time in Figures 12 and 13 for the "solid" draft gear spring constants of Figures 10 and 11, respectively.

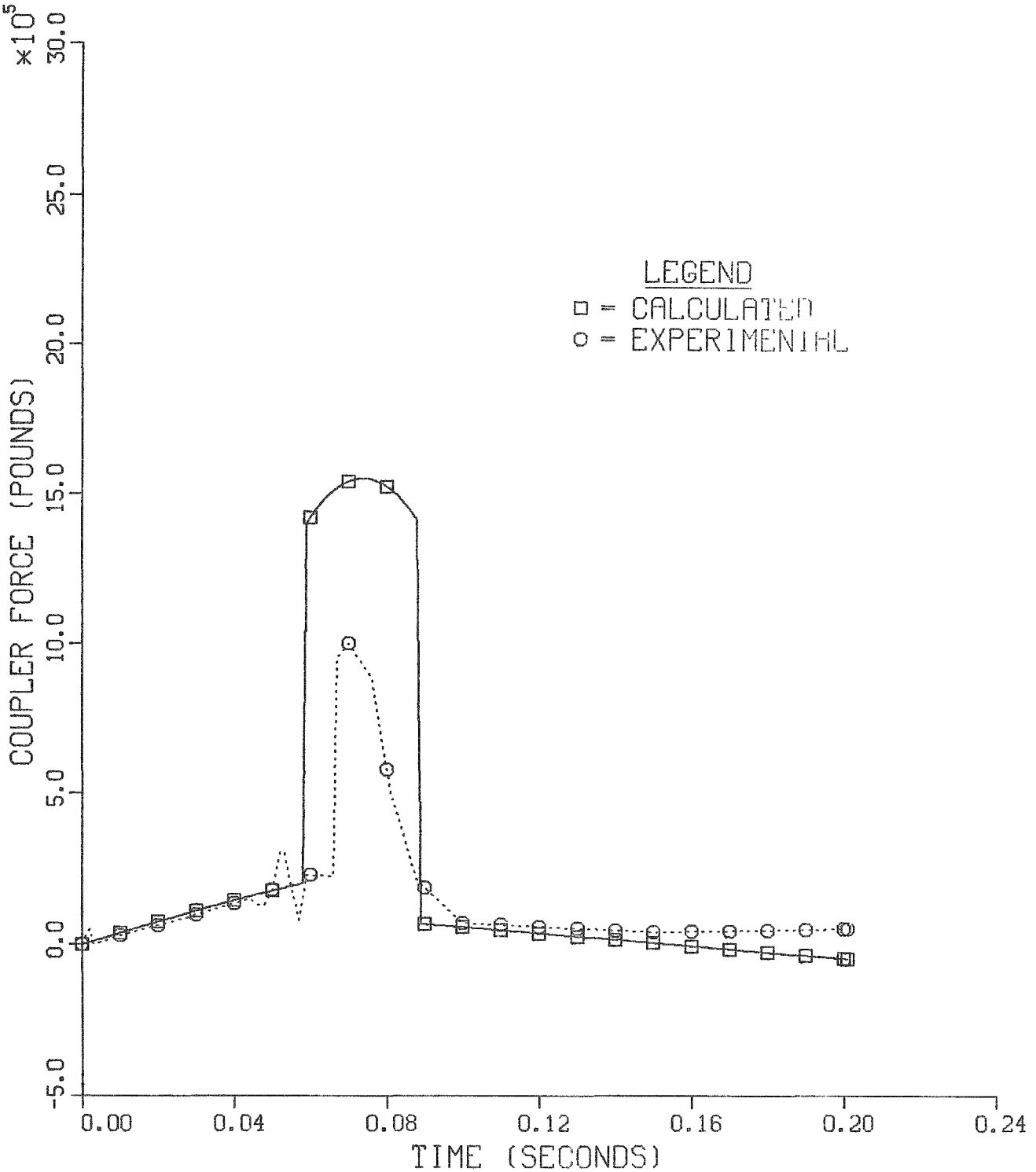

FIGURE 10. Coupler Force vs Time During Impact of Two Hopper Cars Loaded with Gravel (Spring Constant of "Solid" Draft Gears = 5 x 10^5 lbs (force)/inch).

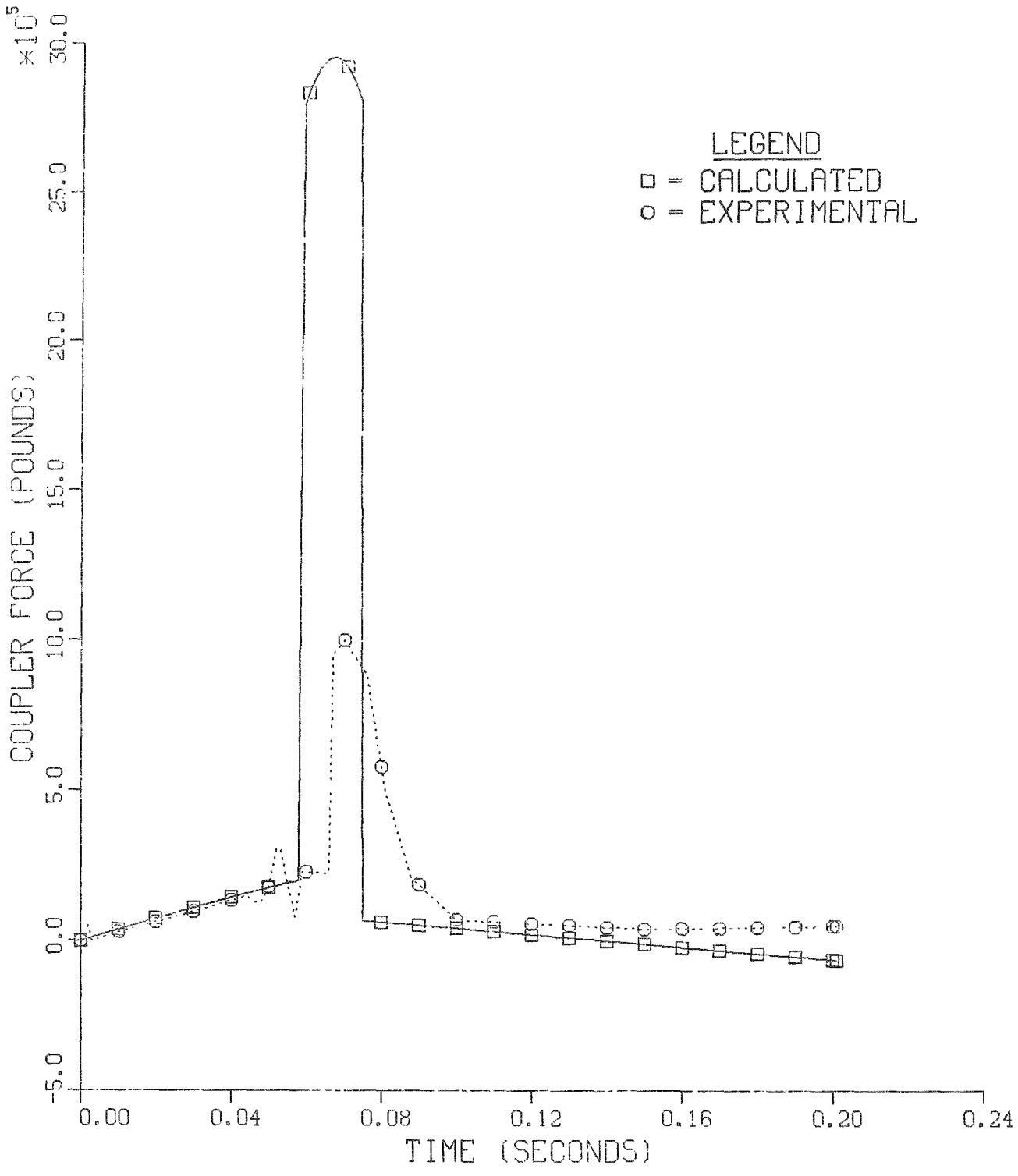

FIGURE 11. Coupler Force vs Time During Impact of Two Hopper Cars Loaded with Gravel (Spring Constant of "Solid" Draft Gears = 1 x 10^6 lbs(force)/inch).

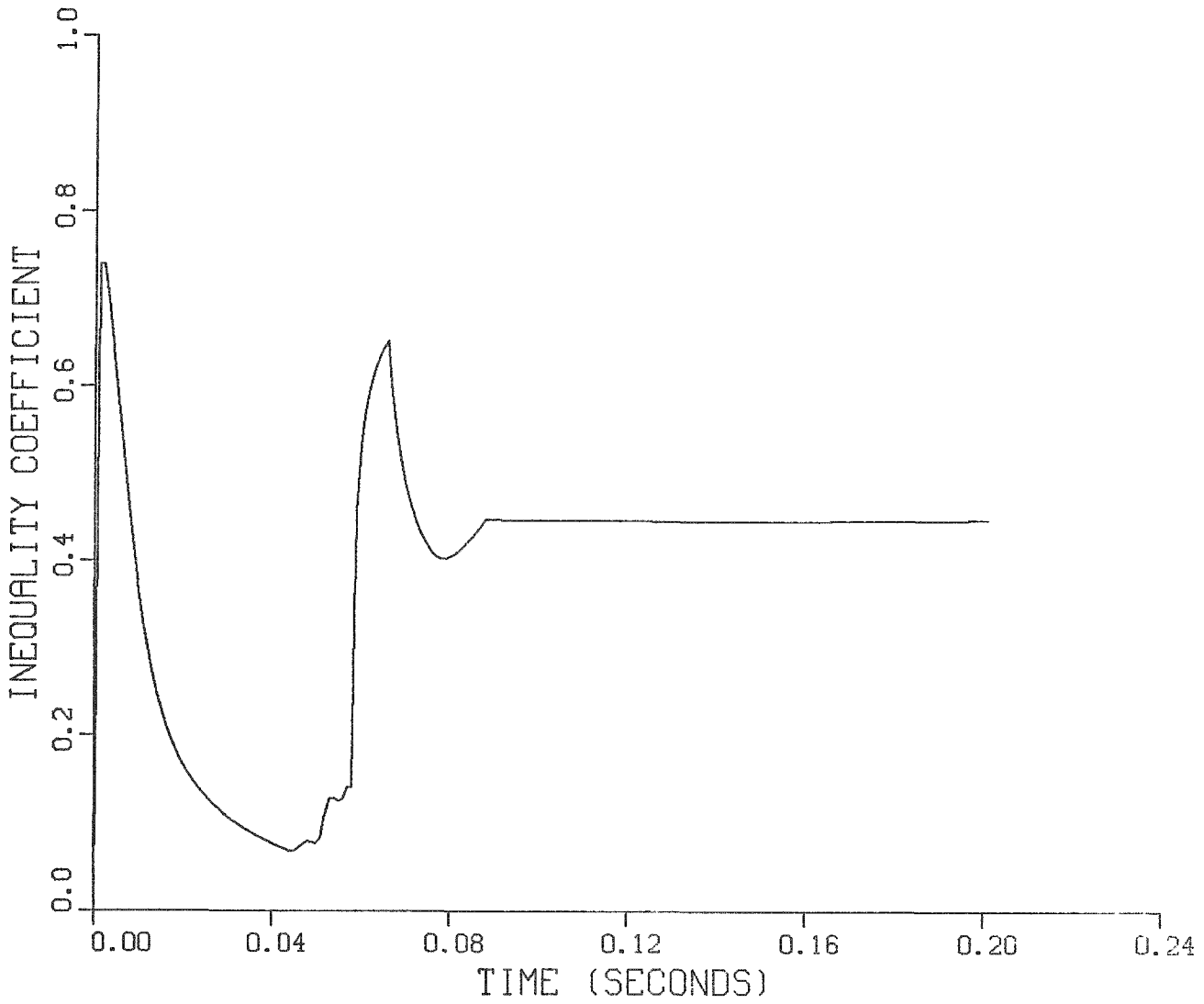

FIGURE 12. Comparison of Calculated and Measured Coupler Force Using Theil's Inequality Coefficient as a Figure of Merit (Spring Constant of "Solid" Draft Gears = 5 x 10^5 lbs(force)/inch).

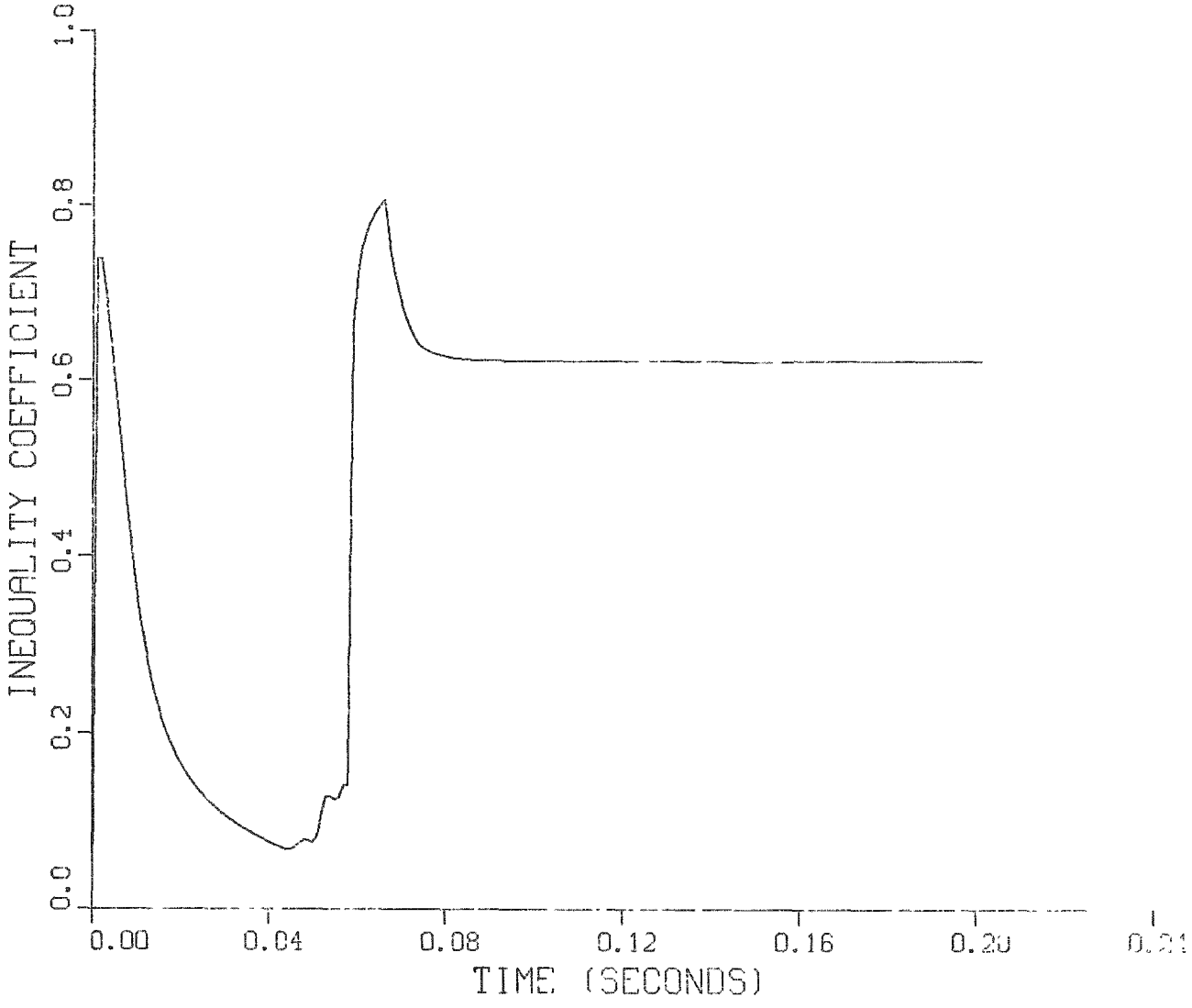

FIGURE 13. Comparison of Calculated and Measured Coupler Force Using Theil's Inequality Coefficient as a Figure of Merit (Spring Constant of "Solid" Draft Gears = 1 x 10^6 lbs(force)/inch).

Two sets of additional simulation runs were made to arrive at the lowest value possible for TIC (signifying the best possible agreement). In the first set, the value of the "solid" draft gear spring constant or stiffness coefficient was held constant throughout a simulation run, but a different value was used for each run in the set. Values of the spring constants used in this set of runs were 2.0×10^5, 2.5×10^5, 3.0×10^5, 4.0×10^5 and 7.5×10^5 lbs (force)/inch. TIC as a function of "solid" draft gear spring constant is presented in Figure 14 and Table 3. The results in Figure 14 and Table 3 show that the minimum final TIC is obtained for a spring constant of 3×10^5 lbs(force)/inch. The calculated coupler force for this case, as a function of time during impact, is compared with the experimental data of Baillie[5] in Figure 15. The calculated time-varying TIC is presented in Figure 16. The results of Figure 15 show that the calculated peak coupler force is very close to that obtained during the impact test, but the area under the force-time curve during the "solid" state is about twice that for the experimental data. Also, the additional amount of travel, i.e., the difference between the horizontal displacement of the hammer car (X_{RC}) and that of the anvil car (X_F), for this condition is about 1.0 inch (see Table 3). Dividing this travel equally between the two cars and their gears implies that each combination has deflected (or deformed) about 0.5 inch while the draft gears were in their "solid" state. Maximum values of TIC obtained during the draft gear "solid" state are also presented in Figure 14 and Table 3. The maximum TIC for a solid draft gear spring constant of 2.0×10^5 lbs(force)/inch is lower than that for the spring constant of 3.0×10^5 lbs(force)/inch, but the "goodness" of agreement between the model and the experiment is based on the final or overall value of TIC, which is lower for the latter spring constant.

In the second set of additional simulation runs made to determine the lowest value of TIC, the "solid" draft gear spring constants were allowed to vary as functions of the relative displacement

$$X_T = X_{RC} - X_F \tag{6}$$

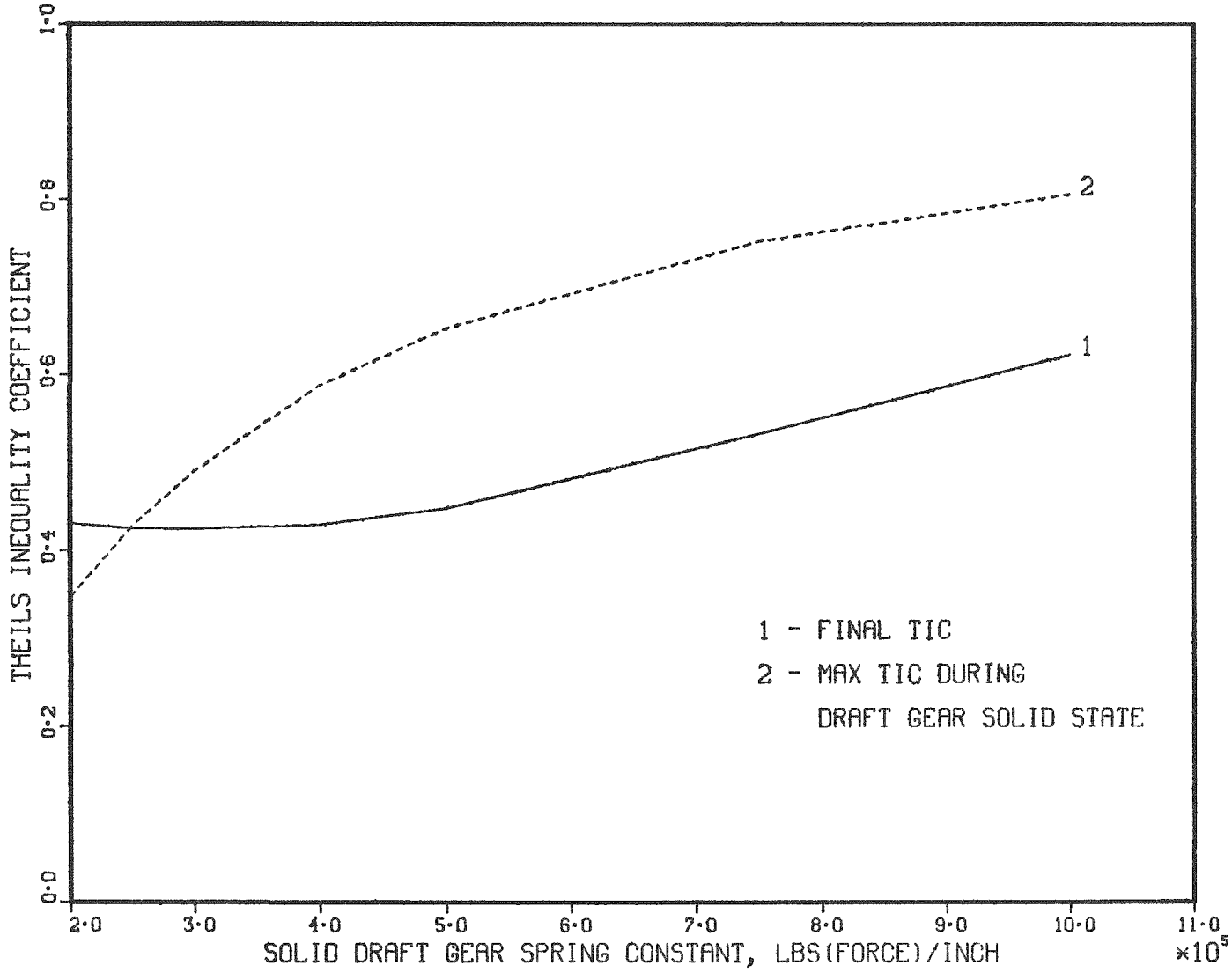

FIGURE 14. Theil's Inequality Coefficient as a Function of "Solid" Draft Gear Spring Constant.

TABLE 3

COMPARISON OF CALCULATED AND MEASURED VALUES OF COUPLER FORCE USING THEIL's INEQUALITY COEFFICIENT AS A FIGURE OF MERIT (CONSTANT "SOLID" DRAFT GEAR SPRING CONSTANT FOR EACH CASE)

"Solid" Draft Gear Spring Constants K_{SDG1}, K_{SDG2} lbs(force)/inch	Figure of Merit, Theil's Inequality Coefficient, TIC				Maximum Coupler Force lbs(force)		Amount of Draft Gear Travel or Deformation During "Solid" State (X_T > 5.6 inches) in Inches
	Minimum	Maximum	Maximum in "solid" state	Final or Overall	Calculated	Experimental	
2.0×10^5	0.0684	0.74	0.347	0.431	0.7×10^6	1×10^6	1.41
2.5×10^5	↓	↓	0.428	0.425	0.844×10^6	↓	1.15
3.0×10^5	↓	↓	0.49	0.424	0.986×10^6	↓	0.971
4.0×10^5	↓	↓	0.588	0.429	1.27×10^6	↓	0.742
5.0×10^5	↓	↓	0.653	0.448	1.55×10^6	↓	0.600
7.5×10^5	↓	↓	0.752	0.533	2.25×10^6	↓	0.407
$10. \times 10^5$	0.0684	0.74	0.806	0.623	2.95×10^6	1×10^6	0.307

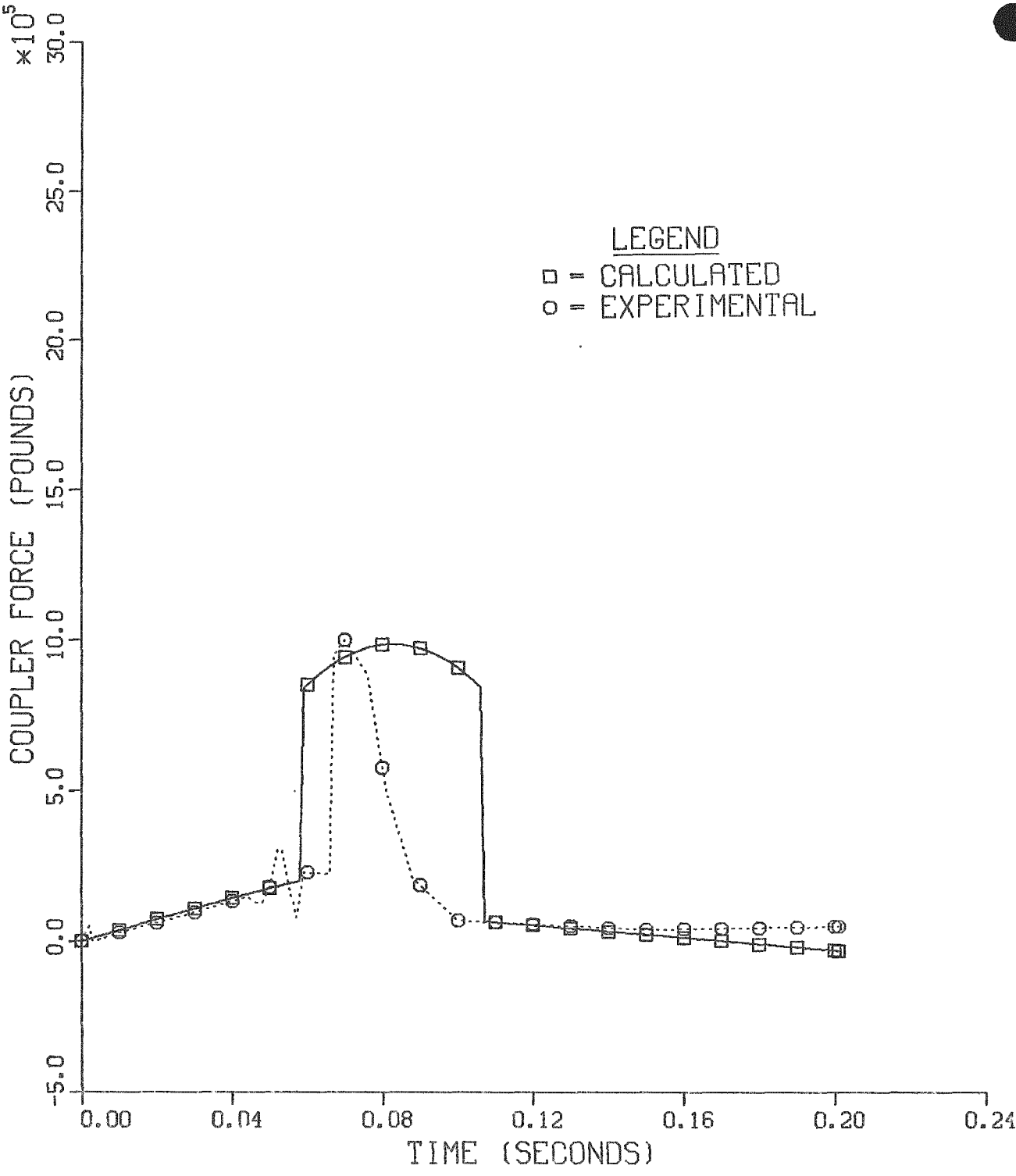

FIGURE 15. Coupler Force vs Time During Impact of Two Hopper Cars Loaded with Gravel (Spring Constant of "Solid" Draft Gears = 3 x 10^5 lbs(force)/inch).

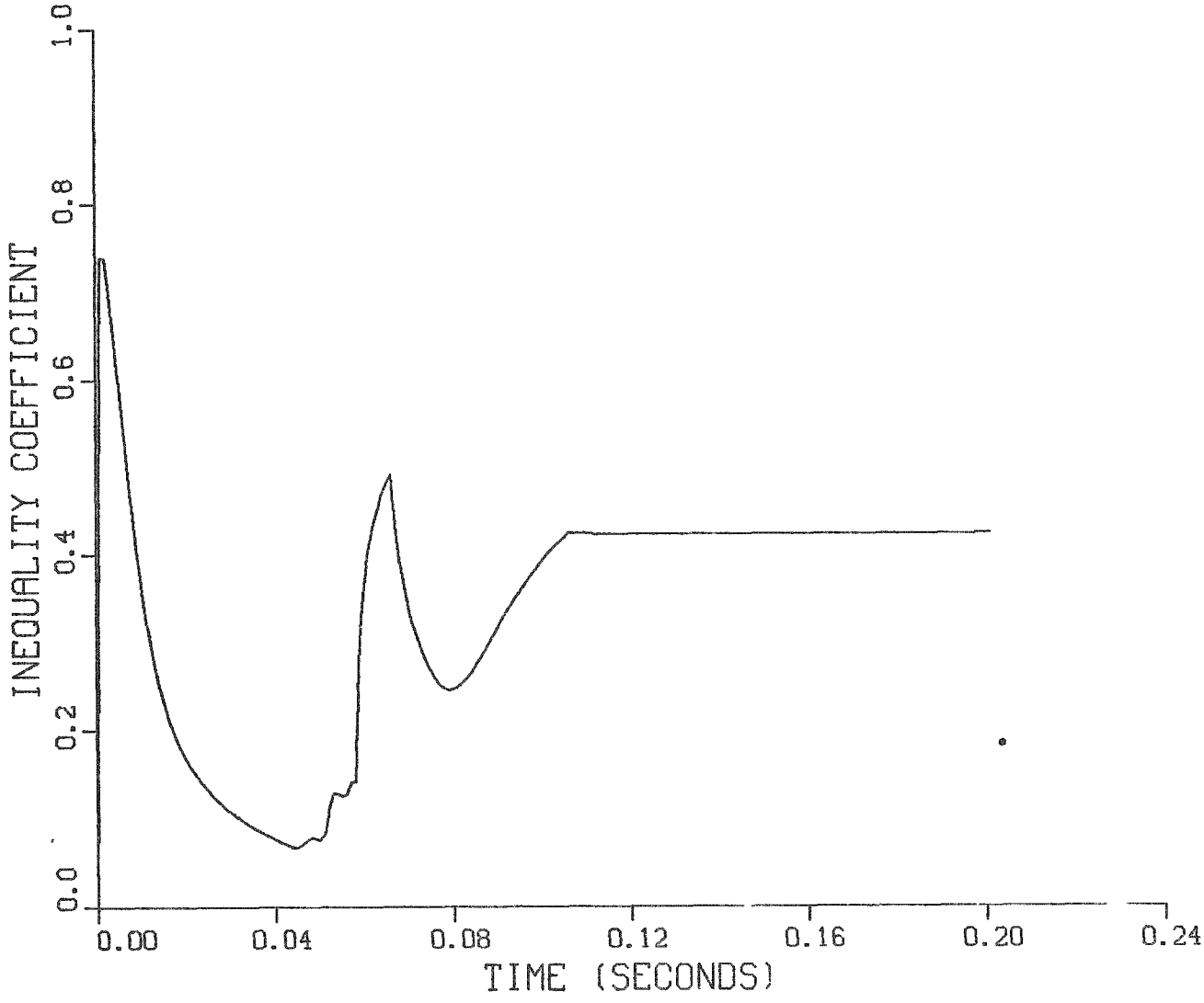

FIGURE 16. Comparison of Calculated and Measured Coupler Force Using Theil's Inequality Coefficient as a Figure of Merit (Spring Constant of "Solid" Draft Gears = 3 x 10^5 lbs(force)/inch).

beyond the maximum value of X_T for the "active" state. The spring constants increased in magnitude as X_T increased beyond this "active" limit. The spring constants were expressed as the products of pre-selected reference values and a multiplying factor which varied as a function of X_T beyond its active limit.

$$K_{SDG1} = K_{SDG10}\phi(X_T) \tag{7}$$

$$K_{SDG2} = K_{SDG20}\phi(X_T) \tag{8}$$

where

K_{SDG1}, K_{SDG2} = the spring constants of the "solid" draft gears on the hammer and anvil cars, respectively, lbs(force)/inch

K_{SDG10}, K_{SDG20} = reference spring constants corresponding to K_{SDG1} and K_{SDG2}, respectively, lbs(force)/inch

$\phi(X_T)$ = a multiplying factor. A function of X_T, i.e.,

$\phi(X_T) = 1.0$ when $X_T = 5.6$ inches
$\phi(X_T) > 1.0$ when $X_T > 5.6$ inches.

The lower limit imposed on the reference values was the value of the "active" state spring constant. The lower limit imposed on the multiplying factor was 1.0, and the upper limit was an extrapolation from the value set for X_T of 6.35 inches. Results obtained for this set of runs are presented in Table 4 as functions of the reference spring constants and the multiplying factor for X_T of 6.35 inches. The lowest final value of TIC in Table 4 is 0.424, which corresponds to a reference spring constant of 1.0×10^5 lbs(force)/inch and a multiplying factor of 4.0. The calculated peak coupler force for this condition is 1.83×10^6 lbs(force), compared to the experimental peak

TABLE 4

COMPARISON OF CALCULATED AND MEASURED VALUES OF COUPLER FORCE USING THEIL's INEQUALITY COEFFICIENT AS A FIGURE OF MERIT ("SOLID" DRAFT GEAR SPRING CONSTANT A FUNCTION OF DRAFT GEAR TRAVEL, X_T)

"Solid" Draft Gear Spring Constants K_{SDG1}, K_{SDG2} lbs(force)/inch	Value of Multiplier Function $\phi(X_T)$ at X_T = 6.35 inches	Figure of Merit, Theil's Inequality Coefficient, TIC				Maximum Coupler Force lbs(force)		Amount of Draft Gear Travel or Deformation During "Solid" State (X_T >5.6 inches) in Inches
		Minimum	Maximum	Maximum in "solid" state	Final or Overall	Calculated	Experimental	
0.75×10^5	4	0.0684	0.74	0.437	0.437	1.63×10^6	1.0×10^6	1.15
1.0×10^5	4	0.0684	0.74	0.424	0.424	1.83×10^6	1.0×10^6	1.004
1.0×10^5	5	0.0684	0.74	0.436	0.436	2.24×10^6	1.0×10^6	0.934
2.0×10^5	5	0.0684	0.74	0.557	0.457	2.77×10^6	1.0×10^6	0.689

force of about 1.0×10^6 lbs(force). The spring constant for a single "solid" draft gear varied from a minimum of 1.0×10^5 lbs(force)/inch to a maximum of 5.52×10^5 lbs(force)/inch (the spring constant for the combined draft gears varied from about 5×10^4 to 2.76×10^5 lbs(force)/ inch). The additional amount of draft gear travel for this "solid" state condition is about 1.0 inch. The calculated coupler force for this case, as a function of time during impact, is compared with experimental data in Figure 17, and the time-varying TIC is presented in Figure 18.

The following comparisons may be made between the "best" runs from each set. The lowest TIC for both sets of runs was 0.424. The maximum TIC during the "solid" state of the draft gear was 0.49 in the first set (Table 3) and 0.424 (the same as the final value) in the second set (Table 4). The first set of runs produced a peak coupler force of 9.86×10^5 lbs(force) compared to a peak value of 1.83×10^6 lbs(force) for the second set. Finally, the additional amount of travel of the combined gears after bottoming out is 0.971 inch for the first set and 1.004 inches for the second set. The greatest difference between the two sets is in the peak coupler force. The first set produced a peak force closer to that of the experimental data, but its duration is greater and it does not have the characteristic shape of the experimental curve. On the other hand, the second set follows the characteristic shape, but both its magnitude and duration are larger than those of the experimental curve.

A maximum value of TIC of about 0.74 is common to Figures 12, 13, 16 and 18. This is due to a perturbation in the experimental data during the first 0.002 second after impact (see Figures 10, 11, 15 and 17). Experimental data indicate that the coupler force rises from 0 to a value of about 50,000 lbs(force) at 0.002 second after impact, and then drops back to 0 during the following 0.001 second. The calculated coupler force varies gradually during this period. Consequently, due to the wide differences in the calculated and experimental coupler forces and the small number of data points for comparison, the TIC calculated for this period reflects the poor initial agreement

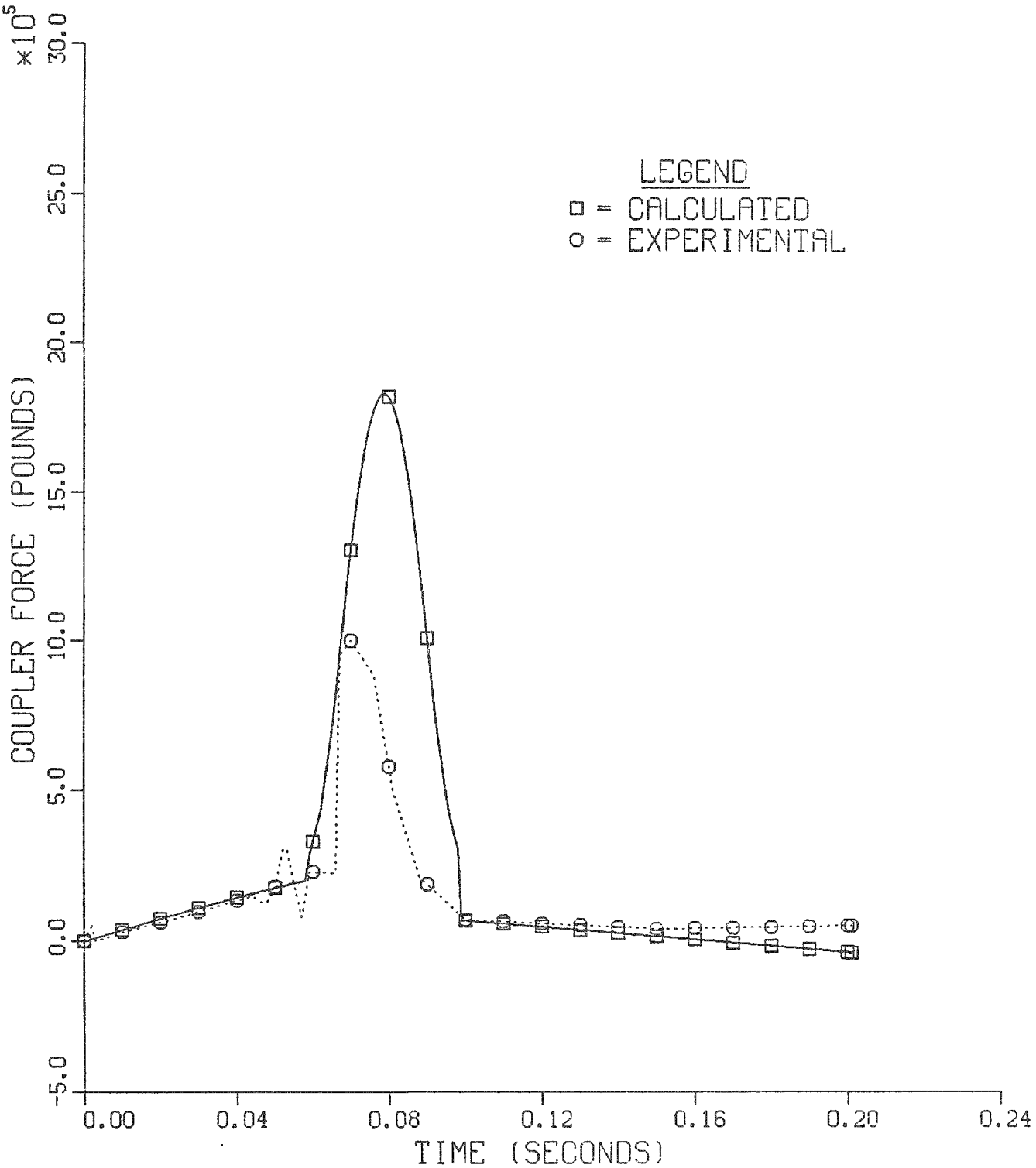

FIGURE 17. Coupler Force vs Time During Impact of Two Hopper Cars Loaded with Gravel ("Solid" Draft Gear Spring Constant a Function of Draft Gear Travel, X_T).

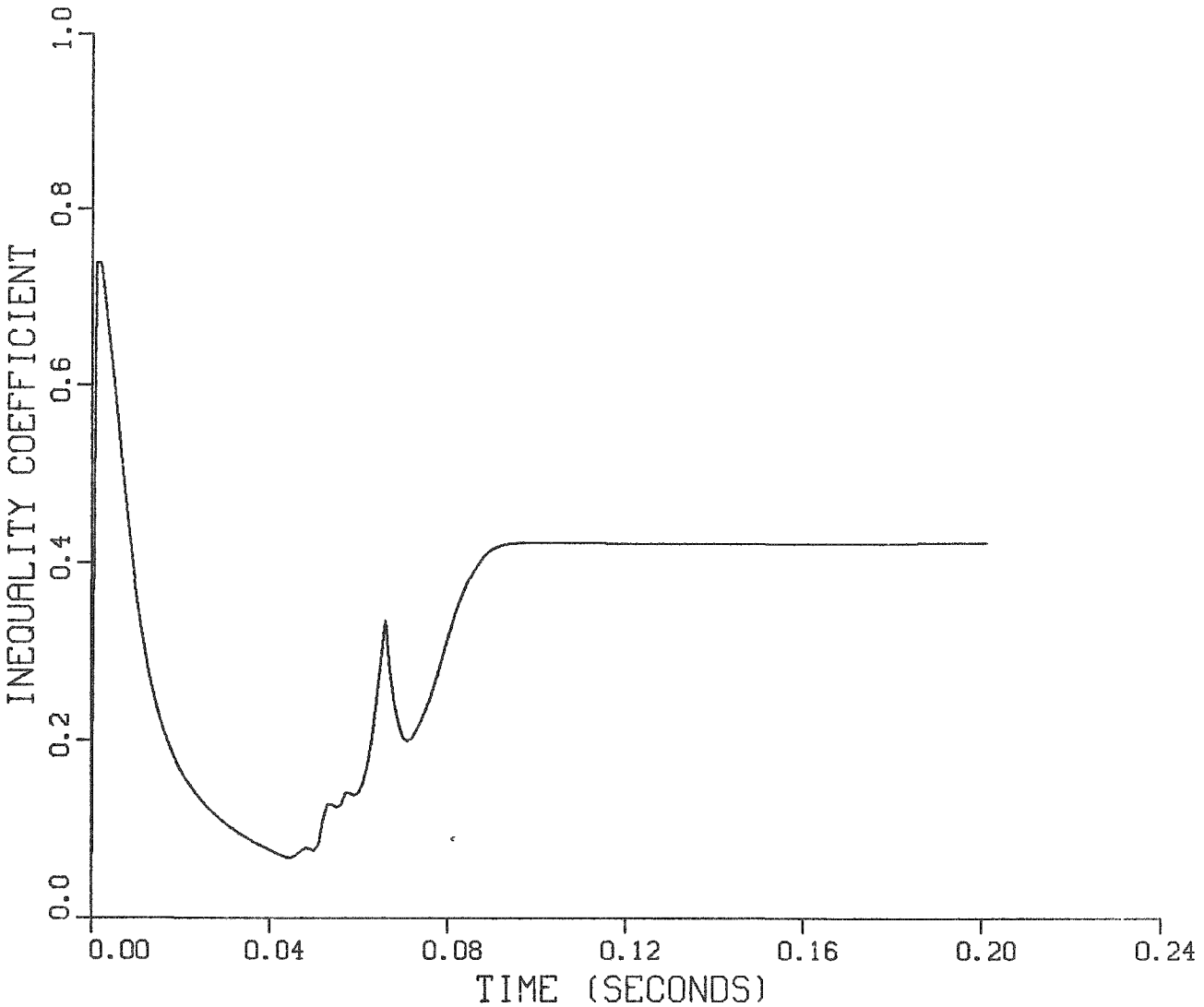

FIGURE 18. Comparison of Calculated and Measured Coupler Force Using Theil's Inequality Coefficient as a Figure of Merit ("Solid" Draft Gear Spring Constant a Function of Draft Gear Travel, X_T).

between the model output and experimental data. Further examination of Figures 12, 13, 16 and 18 shows a quick recovery as TIC drops to its lowest value (best agreement) of about 0.0684 just before the next major perturbation in experimental data at about 0.053 second. This perturbation causes a short sharp rise in TIC followed by a short recovery period. The draft gears then bottom out and large differences between experimental and calculated values of coupler force during the draft gears' "solid" state result in an increasing value of TIC. TIC then recovers to some extent and levels off at a final value between 0.42 and 0.45 when the draft gears re-enter their "active" state.

Closer agreement between model results and experimental data for the "solid" state portion of the transient might be possible by accounting for dissipation of a portion of the total kinetic energy of the system due to cargo shifting and/or deformation relative to the rail cars. Investigation of these mechanisms will be considered as the study progresses. Emphasis will be placed on defining a car to car characterization factor or function which will be used in lieu of attempting to model each car in a train in detail. A characterization function approach is important since the make-up of an anvil train could vary considerably.

4. Collect Parameter Data

There has been no activity in this task during this reporting period.

5. Parametric and Sensitivity Analysis

A parametric and sensitivity analysis was initiated to identify those parameters which significantly affect the normal shock and vibration environment and the response of the cask-rail car system.

In the analysis of dynamic systems it is often necessary to determine system response characteristics, not only for selected operating conditions

(base case), but also for a range of conditions over which certain system parameters can vary. If the system is described in terms of a set of differential equations

$$\frac{d^2X_i}{dt^2} = f_i\left(X_1, X_2, \ldots, \frac{dX_1}{dt}, \frac{dX_2}{dt}, \ldots, t; \alpha_1, \alpha_2, \ldots\right)$$

$$i = 1, 2, \ldots, \qquad (9)$$

where $\alpha_1, \alpha_2, \ldots, \alpha_m$ are system parameters of particular interest, then any information obtained from the solution of this set of equations which contributes to a knowledge of the system response as a function of these parameters will be valuable. Let the solution of Equation (9) for a prescribed set of parameters and initial conditions be expressed as

$$X_{io} = X_{io}\left(t; \alpha_1, \alpha_2, \ldots.\right) \qquad i = 1, 2, \ldots., n \quad . \qquad (10)$$

The partial derivatives,

$$\frac{\partial X_{io}}{\partial \alpha_1}, \frac{\partial X_{io}}{\partial \alpha_2}, \ldots., \frac{\partial X_{io}}{\partial \alpha_m} \qquad i = 1, 2, \ldots. n \qquad (11)$$

referred to as parameter influence coefficients, provide valuable information on system response as a function of the parameters. They can be used to predict system performance in the neighborhood of the known solution X_{io} by first-order approximation, and to describe system sensitivity to certain changes. In a parametric study of the system, the parameter influence coefficients help to reduce the number of computer runs and provide insight into trends of performance and the identification of critical parameters.

Two approaches to the parametric and sensitivity analysis are being considered. The first method is based on the computation of time-varying parameter influence coefficients, TPIC, (partial derivatives of a system

output response variable with respect to a system parameter) during a simulation, using sets of differential equations derived from the equations of motion.[6] Another method is based on an Algebraic Monte Carlo (AMC) technique in which the influence of each parameter on selected output or response variables is determined by varying the parameters one at a time, over their ranges of uncertainty, while holding all other parameters constant. In the AMC method, a curve is plotted which represents the effect of a parameter on the response variables, an equation is fitted to the curve, and the equation is then differentiated with respect to the parameter to arrive at the influence coefficient.

The TPIC technique is a method for obtaining parameter influence coefficients by solving a set of auxiliary differential equations, known as sensitivity equations, simultaneously with the original system equations. The sensitivity equations are derived from the original equations by differentiation and then added to the set of equations already programmed into the system model. This means that parameter influence coefficients are obtained at the expense of greater model complexity. However, the advantages of this trade-off are judged to be well worth the increased complexity.

The TPIC method has been tested using the CARDT model. CARDT was also used during this reporting period to test a model validation algorithm (see Section 3). In the TPIC method, the differential equations for the influence coefficients (sensitivity equations), derived from the equations of motion and auxiliary equations of the model, are "slaved" to the equations of motion ("master" equations) and the two sets of equations are solved simultaneously during the simulation. As an example, consider one of the equations of motion from the CARDT model,

$$\frac{d^2 X_{RC}}{dt^2} = - \frac{K_T}{M_{RC}} (X_{RC} - X_F) \qquad (12)$$

and its initial conditions

$$\left.\begin{aligned} X_{RC}(0) &= 0 \\ \frac{dX_{RC}(0)}{dt} &= V_{XRCI} \end{aligned}\right\} \qquad (13)$$

where

M_{RC} = the mass of the hammer car, $\frac{\text{lbs(force)-sec}^2}{\text{inches}}$

K_T = the total equivalent spring constant for the combined draft gears of the hammer car and the anvil car, lbs(force)/inch (See Reference 1.)

V_{XRCI} = the initial velocity of the hammer car, inches/second.

To determine the influence of the input parameter M_{RC} on the response variable X_{RC}, Equation (12) is differentiated* with respect to M_{RC}

$$\frac{\partial^3 X_{RC}}{\partial M_{RC}\,\partial t^2} = -\frac{K_T}{M_{RC}}\left(\frac{\partial X_{RC}}{\partial M_{RC}} - \frac{\partial X_F}{\partial M_{RC}}\right) + \frac{K_T}{M_{RC}^2}(X_{RC} - X_F) \quad . \qquad (14)$$

Setting

$$IC1 = \frac{\partial X_{RC}}{\partial M_{RC}} \qquad (15)$$

and

$$IC2 = \frac{\partial X_F}{\partial M_{RC}} \qquad (16)$$

*Since X_{RC} is a function of both M_{RC} and time t, partial differentiation is indicated.

and differentiating Equation (15) twice with respect to time gives

$$\frac{d(IC1)}{dt} = \frac{\partial^2 X_{RC}}{\partial M_{RC} \partial t} \tag{17}$$

$$\frac{d^2(IC1)}{dt^2} = \frac{\partial^3 X_{RC}}{\partial M_{RC} \partial t^2} \quad . \tag{18}$$

Replacing terms in Equation (14) with their equivalents from Equations (15), (16), and (18), transforms Equation (14) into the sensitivity equation

$$\frac{d^2(IC1)}{dt^2} = -\frac{K_T}{M_{RC}} (IC1-IC2) + \frac{K_T}{M_{RC}^2} (X_{RC}-X_F) \quad . \tag{19}$$

Differentiation of the initial conditions (13) yields the following initial conditions for Equation (19)

$$\left.\begin{aligned} \frac{\partial X_{RC}(0)}{\partial M_{RC}} &= IC1(0) = 0 \\ \text{and} \quad \frac{\partial^2 X_{RC}(0)}{\partial M_{RC} \partial t} &= \frac{dIC1}{dt}(0) = 0 \end{aligned}\right\} \quad . \tag{20}$$

The influence coefficient IC1 is obtained by the simultaneous solution of Equations (12) and (19). The "driver" or "master" equation is Equation (12), and the "driven" or "slave" equation is Equation (19). These two equations are coupled together by the variables X_{RC} and X_F.

The influence coefficient IC2 is obtained using this same procedure for the equation of motion

$$\frac{d^2X_F}{dt^2} = \frac{K_T}{M_{RC}} (X_{RC}-X_F) \quad . \tag{21}$$

The TPIC method was programmed into the CARDT model along with the model validation technique discussed in Section 3. Parameter influence coefficients, determined simultaneously with the determination of Theil's inequality coefficient, are presented in Tables 5 and 6 for two of the several simulation runs described in Section 3. Table 5 presents influence coefficients and the ranking of parameters by influence coefficient for a run based on constant "solid" draft gear stiffnesses (K_{SDG1} and K_{SDG2}) of 3×10^5 lbs(force)/inch (see Table 3 and Figures 15 and 16). Table 6 presents results for a simulation run based on "solid" draft gear stiffnesses that varied as functions of the relative displacement

$$X_T = X_{RC} - X_F \tag{6}$$

beyond the maximum value of X_T for the "active" state. (See Table 4 and Figures 17 and 18). The results of Tables 5 and 6 show that the parameters with the most influence on the response variables F_T, K_T, X_{RC} and X_F during the "active" state of the draft gears are μ_D, a multiplying factor corresponding to a coefficient of friction for the damping device in a draft gear, and the sign function of the relative velocity $DX_T = \frac{dX_T}{dt}$. The parameters which affect F_T the most during the "solid" state of the draft gears are the car masses M_F and M_{RC}. The response variables X_{RC} and X_F are influenced the most during this state by V_{XRCI}, the initial velocity of the hammer car, followed by M_{RC} for X_{RC} and M_F for X_F. The combined draft gear spring constant K_T is influenced equally by the "solid" draft gear spring constants K_{SDG1} and K_{SDG2} during the "solid" state. The maximum travel of the combined draft gears for all cases during the "active" state was set at 5.6 inches.

TABLE 5

RANKING OF PARAMETERS BY PARAMETER INFLUENCE COEFFICIENTS DERIVED FROM SIMULATION RUNS USING THE *CARDT* MODEL

(Constant "Solid" Draft Gear Spring Constants, $K_{SDG1} = K_{SDG2} = 3 \times 10^5$ lbs(force)/inch; Maximum Travel of Combined Draft Gears in "Active" State = 5.6 inches)

Response or Output Variable	Input Parameter	Parameter Influence Coefficient	Range of Parameter Influence Coefficient During Simulation		Input Parameter Rank By Influence Coeff.
			Minimum	Maximum	
Coupler Force, F_T	μ_D	$\frac{\partial F_T}{\partial \mu_D}$ *	-1.43×10^5	1.24×10^5	1
	$Sgn(DX_T)$	$\frac{\partial F_T}{\partial [Sgn(DX_T)]}$ *	-5.16×10^4	6.33×10^4	2
	M_F	$\frac{\partial F_T}{\partial M_F}$	0	616.	3
	M_{RC}	$\frac{\partial F_T}{\partial M_{RC}}$	0	577.	4
	K_1	$\frac{\partial F_T}{\partial K_1}$ *	-1.59	1.91	5
	K_2	$\frac{\partial F_T}{\partial K_2}$ *	-1.59	1.91	5
	K_{SDG1}	$\frac{\partial F_T}{\partial K_{SDG1}}$ **	-0.289	1.53	6
	K_{SDG2}	$\frac{\partial F_T}{\partial K_{SDG2}}$ **	-0.289	1.53	6

* Valid only during "Active" state of draft gears.
**Valid only during "Solid" state of draft gears.

TABLE 5 (Cont'd)

Response or Output Variable	Input Parameter	Parameter Influence Coefficient	Range of Parameter Influence Coefficient During Simulation		Input Parameter Rank By Influence Coeff.
			Minimum	Maximum	
Horizontal Displacement of Hammer Car, X_{RC}	$Sgn\ (DX_T)$	$\frac{\partial X_{RC}^*}{\partial [Sgn(DX_T)]}$	-0.419	0	1
	μ_D	$\frac{\partial X_{RC}^*}{\partial \mu_D}$	-0.339	0.250	2
	V_{XRCI}	$\frac{\partial X_{RC}}{\partial V_{XRCI}}$	0	0.0899	3
	M_{RC}	$\frac{\partial X_{RC}}{\partial M_{RC}}$	0	0.017	4
	M_F	$\frac{\partial X_{RC}}{\partial M_F}$	-0.00341	0	5
	K_{SDG1}	$\frac{\partial X_{RC}^{**}}{\partial K_{SDG1}}$	-1.17×10^{-5}	0	6
	K_{SDG2}	$\frac{\partial X_{RC}^{**}}{\partial K_{SDG2}}$	-1.17×10^{-5}	0	6
	K_1	$\frac{\partial X_{RC}^*}{\partial K_1}$	-7.32×10^{-6}	0	7
	K_2	$\frac{\partial X_{RC}^*}{\partial K_2}$	-7.32×10^{-6}	0	7

TABLE 5 (Cont'd)

Response or Output Variable	Input Parameter	Parameter Influence Coefficient	Range of Parameter Influence Coefficient During Simulation		Input Parameter Rank By Influence Coeff.
			Minimum	Maximum	
Horizontal Displacement of Anvil Car, X_F	$Sgn(DX_T)$	$\frac{\partial X_{RC}^*}{\partial[Sgn(DX_T)]}$	0	0.433	1
	μ_D	$\frac{\partial X_F^*}{\partial \mu_D}$	-0.258	0.350	2
	V_{XRCI}	$\frac{\partial X_F}{\partial V_{XRCI}}$	0	0.115	3
	M_F	$\frac{\partial X_F}{\partial M_F}$	-0.018	0	4
	M_{RC}	$\frac{\partial X_F}{\partial M_{RC}}$	0	0.0033	5
	K_{SDG1}	$\frac{\partial X_F^{**}}{\partial K_{SDG1}}$	0	1.21×10^{-5}	6
	K_{SDG2}	$\frac{\partial X_F^{**}}{\partial K_{SDG2}}$	0	1.21×10^{-5}	6
	K_1	$\frac{\partial X_F^*}{\partial K_1}$	0	7.56×10^{-6}	7
	K_2	$\frac{\partial X_F^*}{\partial K_2}$	0	7.56×10^{-6}	7

TABLE 5 (Cont'd)

Response or Output Variable	Input Parameter	Parameter Influence Coefficient	Range of Parameter Influence Coefficient During Simulation		Input Parameter Rank By Influence Coeff.
			Minimum	Maximum	
Combined Draft Gear Spring Constant, K_T	μ_D	$\frac{\partial K_T^*}{\partial \mu_D}$	-2.43×10^4	2.43×10^4	1
	$Sgn(DX_T)$	$\frac{\partial K_T^*}{\partial [Sgn(DX_T)]}$	0	1.217×10^4	2
	K_1	$\frac{\partial K_T^*}{\partial K_1}$	0	0.375	3
	K_2	$\frac{\partial K_T^*}{\partial K_2}$	0	0.375	3
	K_{SDG1}	$\frac{\partial K_T^{**}}{\partial K_{SDG1}}$	0	0.250	4
	K_{SDG2}	$\frac{\partial K_T^{**}}{\partial K_{SDG2}}$	0	0.250	4

TABLE 6

RANKING OF PARAMETERS BY PARAMETER INFLUENCE COEFFICIENTS DERIVED FROM SIMULATION RUNS USING THE *CARDT* MODEL

("Solid" Draft Gear Spring Constants, $K_{SDG1} = K_{SDG2} = 1.0 \times 10^4$ (Mininum) to 5.52×10^5 (Maximum) lbs(force)/inch;
Maximum Travel of Combined Draft Gears in "Active" State = 5.6 inches)

Response or Output Variable	Input Parameter	Parameter Influence Coefficient	Range of Parameter Influence Coefficient During Simulation		Input Parameter Rank By Influence Coeff.
			Minimum	Maximum	
Coupler Force, F_T	μ_D	$\frac{\partial F_T}{\partial \mu_D}$	-1.52×10^5	1.24×10^5	1
	$Sgn(DX_T)$	$\frac{\partial F_T^*}{\partial [Sgn(DX_T)]}$	-7.61×10^4	6.39×10^4	2
	M_F	$\frac{\partial F_T}{\partial M_F}$	0	456.	3
	M_{RC}	$\frac{\partial F_T}{\partial M_{RC}}$	0	427.	4
	K_1	$\frac{\partial F_T^*}{\partial K_1}$	-2.34	1.91	5
	K_2	$\frac{\partial F_T^*}{\partial K_2}$	-2.34	1.91	5
	K_{SDG1}	$\frac{\partial F_T^{**}}{\partial K_{SDG1}}$	-0.258	1.53	6
	K_{SDG2}	$\frac{\partial F_T^{**}}{\partial K_{SDG2}}$	-0.258	1.53	6

* Valid only during "Active" state of draft gears.
**Valid only during "Solid" state of draft gears.

TABLE 6 (Cont'd)

Response or Output Variable	Input Parameter	Parameter Influence Coefficient	Range of Parameter Influence Coefficient During Simulation		Input Parameter Rank By Influence Coeff.
			Minimum	Maximum	
Horizontal Displacement of Hammer Car, X_{RC}	$Sgn\ (DX_T)$	$\frac{\partial X_{RC}^*}{\partial [Sgn(DX_T)]}$	-0.443	0	1
	μ_D	$\frac{\partial X_{RC}^*}{\partial \mu_D}$	-0.308	0.280	2
	V_{XRCI}	$\frac{\partial X_{RC}}{\partial V_{XRCI}}$	0	0.0867	3
	M_{RC}	$\frac{\partial X_{RC}}{\partial M_{RC}}$	0	0.0179	4
	M_F	$\frac{\partial X_{RC}}{\partial M_F}$	-0.00308	0	5
	K_{SDG1}	$\frac{\partial X_{RC}^{**}}{\partial K_{SDG1}}$	-1.04×10^{-5}	0	6
	K_{SDG2}	$\frac{\partial X_{RC}^{**}}{\partial K_{SDG2}}$	-1.04×10^{-5}	0	6
	K_1	$\frac{\partial X_{RC}^*}{\partial K_1}$	-7.66×10^{-6}	0	7
	K_2	$\frac{\partial X_{RC}^*}{\partial K_2}$	-7.66×10^{-6}	0	7

TABLE 6 (Cont'd)

Response or Output Variable	Input Parameter	Parameter Influence Coefficient	Range of Parameter Influence Coefficient During Simulation		Input Parameter Rank By Influence Coeff.
			Minimum	Maximum	
Horizontal Displacement of Anvil Car, X_F	$Sgn(DX_T)$	$\frac{\partial X_{RC}^*}{\partial [Sgn(DX_T)]}$	0	0.457	1
	μ_D	$\frac{\partial X_F^*}{\partial \mu_D}$	-0.289	0.318	2
	V_{XRCI}	$\frac{\partial X_F^*}{\partial V_{XRCI}}$	0	0.118	3
	M_F	$\frac{\partial X_F}{\partial M_F}$	-0.019	0	4
	M_{RC}	$\frac{\partial X_F}{\partial M_{RC}}$	0	0.00298	5
	K_{SDG1}	$\frac{\partial X_F^{**}}{\partial K_{SDG1}}$	0	1.08×10^{-5}	6
	K_{SDG2}	$\frac{\partial X_F^{**}}{\partial K_{SDG2}}$	0	1.08×10^{-5}	6
	K_1	$\frac{\partial X_F^*}{\partial K_1}$	0	7.91×10^{-5}	7
	K_2	$\frac{\partial X_F^*}{\partial K_2}$	0	7.91×10^{-6}	7

TABLE 6 (Cont'd)

Response or Output Variable	Input Parameter	Parameter Influence Coefficient	Range of Parameter Influence Coefficient During Simulation		Input Parameter Rank By Influence Coeff.
			Minimum	Maximum	
Combined Draft Gear Spring Constant, K_T	μ_D	$\frac{\partial K_T^*}{\partial \mu_D}$	-2.43×10^4	2.43×10^4	1
	$Sgn(DX_T)$	$\frac{\partial K_T^*}{\partial [Sgn(DX_T)]}$	0	1.217×10^4	2
	K_1	$\frac{\partial K_T^*}{\partial K_1}$	0	0.375	3
	K_2	$\frac{\partial K_T^*}{\partial K_2}$	0	0.375	3
	K_{SDG1}	$\frac{\partial K_T^{**}}{\partial K_{SDG1}}$	0	0.250	4
	K_{SDG2}	$\frac{\partial K_T^{**}}{\partial K_{SDG2}}$	0	0.250	4

The results in Table 6 were obtained for a spring constant or stiffness for each single "solid" draft gear that varied from a minimum value of 1.0×10^5 lbs(force)/inch to a maximum value of 5.52×10^5 lbs(force)/inch during the simulation (the stiffness for the combined gears varied from about 5×10^4 to 2.76×10^5 lbs(force)/inch). The stiffnesses increased in magnitude as X_T increased beyond the "active" limit.

Parameter influence coefficients as functions of time are presented in Figures 19 and 20 for the case defined by constant "solid" draft gear spring constants. Figures 21 and 22 show the time-varying influence coefficients for the case defined by variable "solid" draft gear spring constants.

6. INTERIM REPORT

High speed movies made of the coupling action of the rail car, and of the interactions of the rail car, shipping cask, and tiedown mechanism, during the tests conducted at the Savannah River Laboratory in July and August 1978, were transcribed onto a videotape. An annotated version of this tape, "Tests to Study Behavior of a Spent Fuel Shipping Cask-Rail Car System During Humping Operations," was issued and is described in Reference 1.

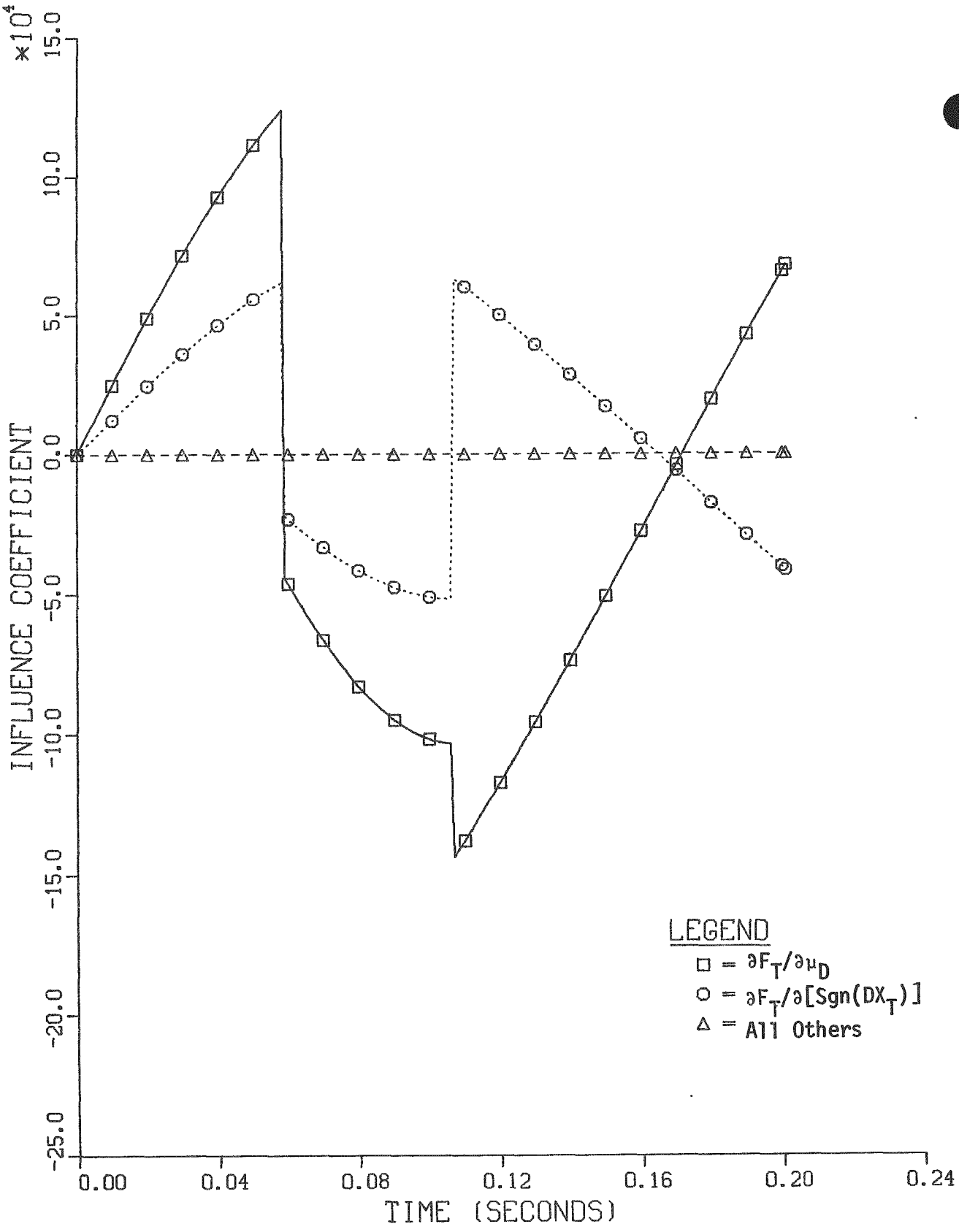

FIGURE 19. Influence of Parameters on Coupler Force (Constant "Solid" Draft Gear Spring Constant = 3 x 10^5 lbs(force)/inch).

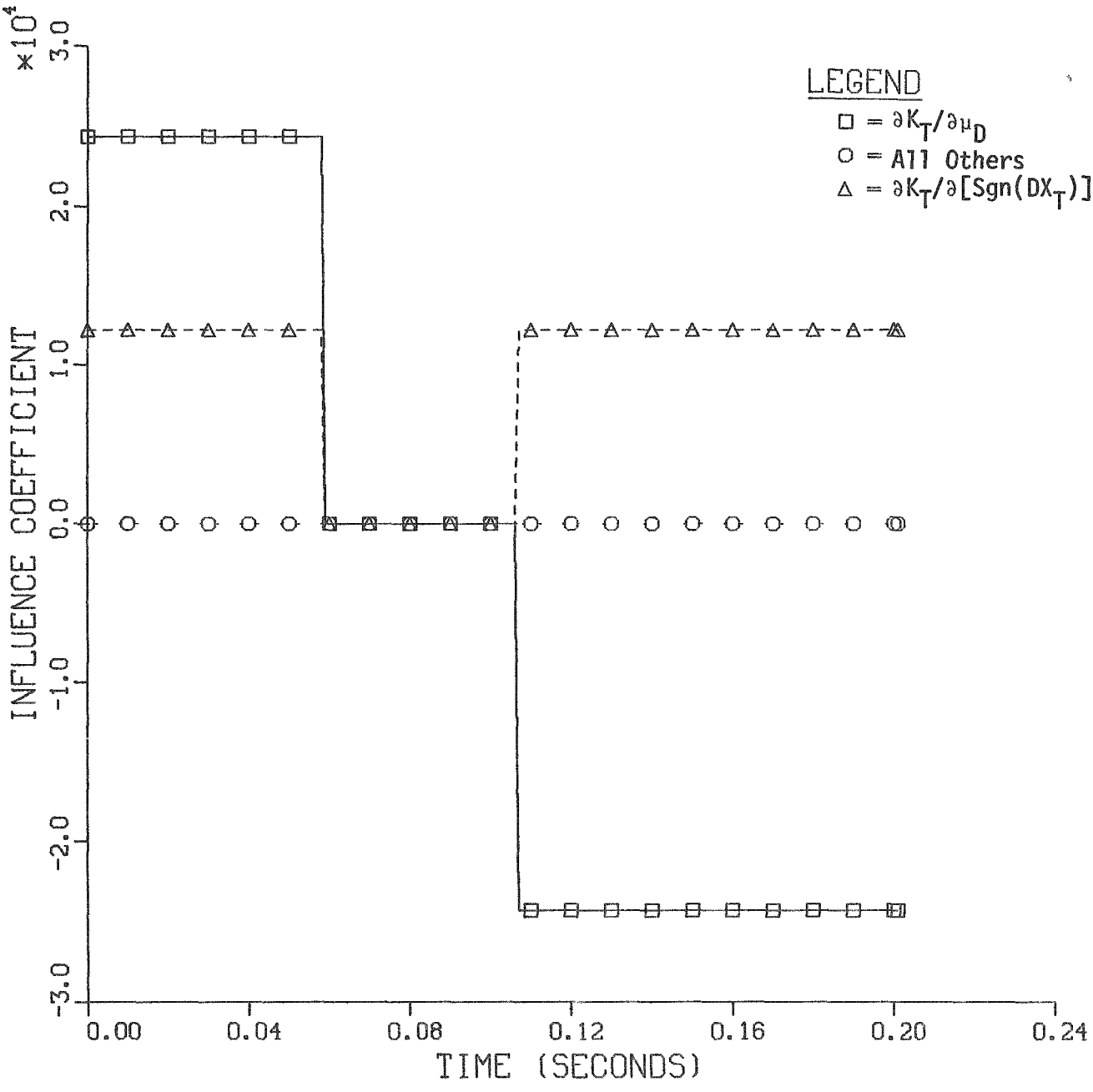

FIGURE 20. Influence of Parameters on the Total Equivalent Spring Constant for the Combined Draft Gears (Constant "Solid" Draft Gear Spring Constant = 3 x 10^5 lbs (force)/inch).

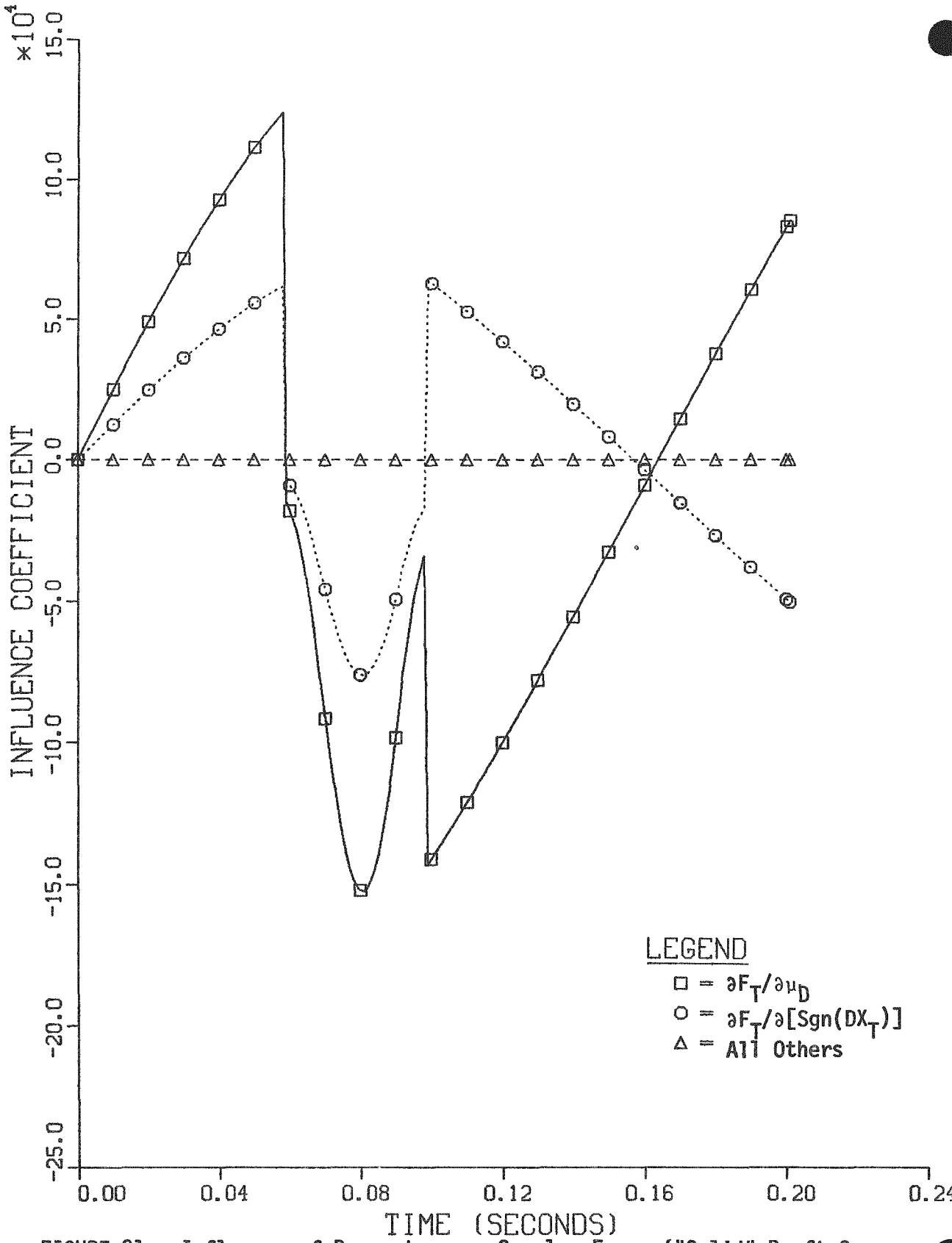

FIGURE 21. Influence of Parameters on Coupler Force ("Solid" Draft Gear Spring Constant a Function of Draft Gear Travel, X_T).

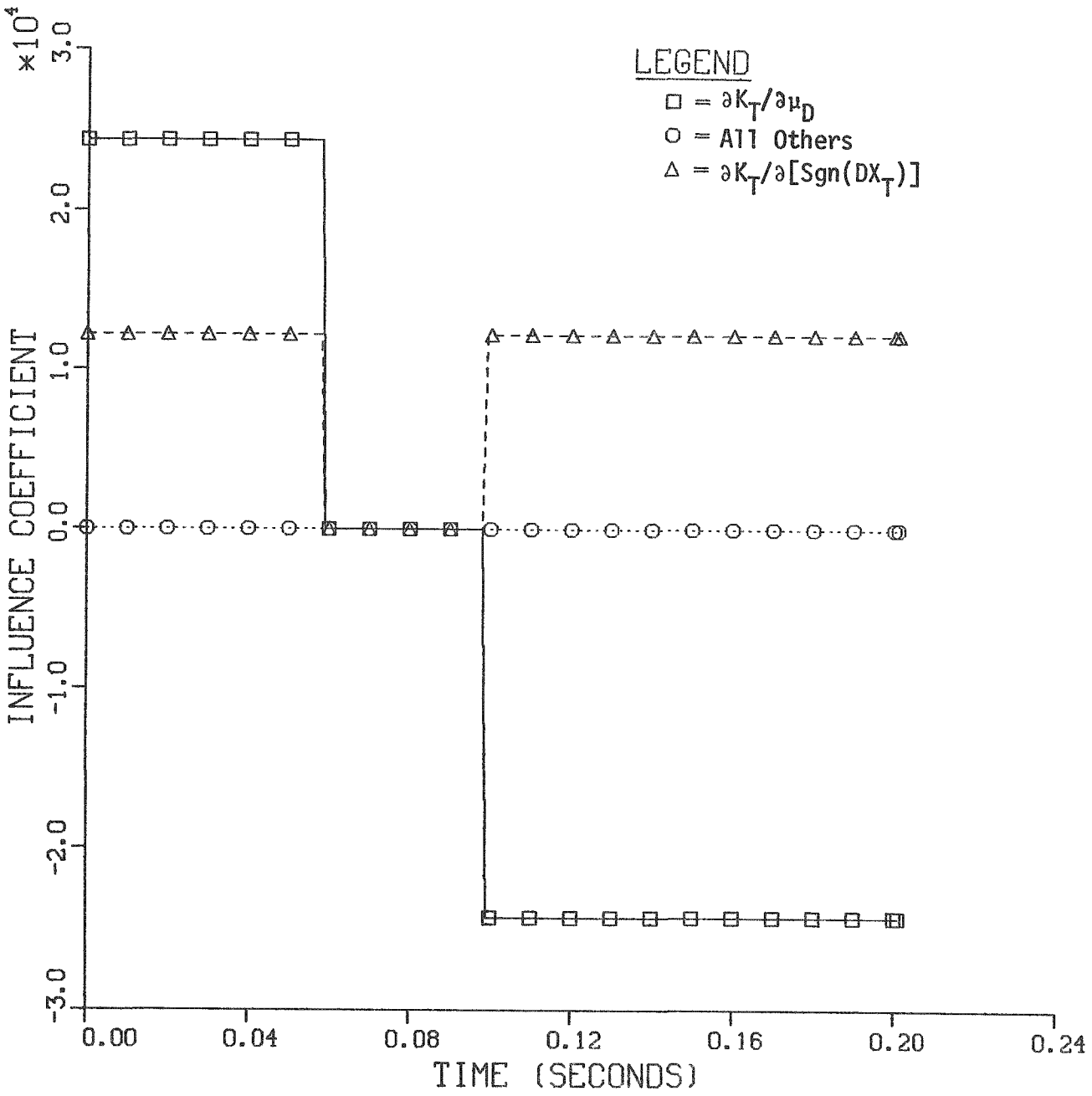

FIGURE 22. Influence of Parameters on the Total Equivalent Spring Constant for the Combined Draft Gears ("Solid" Draft Gear Spring Constant a Function of Draft Gear Travel, X_T).

REFERENCES

1. S. R. Fields and S. J. Mech, "Dynamic Analysis to Establish Normal Shock and Vibration of Radioactive Material Shipping Packages," NUREG/CR-0589 (HEDL-TME 78-102), Quarterly Progress Report (July 1, 1978 - September 30, 1978), November 1978.

2. S. R. Fields and S. J. Mech, "Dynamic Analysis to Establish Normal Shock and Vibration Environments Experienced by Radioactive Material Shipping Packages," NUREG/CR-0161 (HEDL-TME 78-41), Quarterly Progress Report (January 1, 1978 - March 31, 1978), July 1978.

3. N. A. Kheir and W. M. Holmes, "On Validating Simulation Models of Missile Systems," Simulation, April 1978.

4. S. R. Fields and S. J. Mech, "Dynamic Analysis to Establish Normal Shock and Vibration of Radioactive Material Shipping Packages," NUREG/CR-0766 (HEDL-TME 79-3), Quarterly Progress Report (October 1, 1978- December 31, 1978), February 1979.

5. W. E. Baillie, "Impact as Related to Freight Car and Lading Damage," ASME Paper 59-A-249.

6. H. F. Meissinger, "The Use of Parameter Influence Coefficients in Computer Analysis of Dynamic Systems," Simulation, August 1964.

SUPPLEMENTAL DISTRIBUTION LIST
FOR CY-1979 NRC REPORTS
SUBMITTED UNDER SHIPPING CASK DYNAMIC ANALYSIS TASK,
FIN-B2263-8

DOE/Richland Operations (4)
P. O. Box 550
Richland, WA 99352

Chief Patent Attorney
B. J. Melton
J. D. White (2)

DOE/FFTF Project Office
P. O. Box 550
Richland, WA 99352

Director

DOE Chicago Patent Office
9800 S. Cass Avenue
Argonne, IL 60439

A. A. Churm

DOE Environmental Control and Technology Division
Washington, DC 20545

J. Counts

E. I. DuPont de Nemours and Company
P. O. Box A
Aiken, SC 29801

S. F. Petry

Hanford Engineering Development Laboratory (35)
P. O. Box 1970
Richland, WA 99352

Supervisor, Document Processing W/C-123

Los Alamos Scientific Laboratory
P. O. Box 1663
Los Alamos, NM 87545

T. D Butler

Pacific Northwest Laboratory
P. O. Box 999
Richland, WA 99352

L. D. Williams

Sandia Laboratories
P. O. Box 5800
Albuquerque, NM 87115

C. F. Magnuson